

VOLUME 79

SEPARATE No. 330

# PROCEEDINGS

AMERICAN SOCIETY  
OF  
CIVIL ENGINEERS

NOVEMBER, 1953



## PLASTIC DEFORMATION OF WIDE-FLANGE BEAM-COLUMNS

by Robert L. Ketter and Edmund L. Kaminsky,  
Junior Members, ASCE, and  
Lynn S. Beedle, A.M. ASCE

Presented at  
New York City Convention  
October 19-22, 1953

ENGINEERING MECHANICS DIVISION

*{Discussion open until March 1, 1954}*

*Copyright 1953 by the AMERICAN SOCIETY OF CIVIL ENGINEERS  
Printed in the United States of America*

Headquarters of the Society  
33 W. 39th St.  
New York 18, N. Y.

PRICE \$0.50 PER COPY

**THIS PAPER**

--represents an effort of the Society to deliver technical data direct from the author to the reader with the greatest possible speed. To this end, it has had none of the usual editing required in more formal publication procedures.

Readers are invited to submit discussion applying to current papers. For this paper the final closing dead line appears on the front cover.

Those who are planning papers or discussions for "Proceedings" will expedite Division and Committee action measurably by first studying "Publication Procedure for Technical Papers" (Proceedings — Separate No. 290). For free copies of this Separate—describing style, content, and format—address the Manager, Technical Publications, ASCE.

Reprints from this publication may be made on condition that the full title of paper, name of author, page reference, and date of publication by the Society are given.

The Society is not responsible for any statement made or opinion expressed in its publications.

This paper was published at 1745 S. State Street, Ann Arbor, Mich., by the American Society of Civil Engineers. Editorial and General Offices are at 33 West Thirty-ninth Street, New York 18, N. Y.

## PLASTIC DEFORMATION OF WIDE-FLANGE BEAM-COLUMNS

Robert L. Ketter,\* Edmund L. Kaminsky\*\* and Lynn S. Beedle\*\*\*

### I. Synopsis

Presented in this paper are the results of an analytical and experimental study of the inelastic deformations of wide-flange steel beam-columns. Emphasis has been directed toward the influence of axial thrust on the moment-curvature ( $M-\phi$ ) relationship when stresses exceed the elastic limit. The analysis is extended to include the influence of residual stresses, and thus the moment-curvature relationship is developed as a function of axial thrust and residual stress. Buckling loads are then determined for eccentrically loaded steel columns of WF shape, the necessity for an assumed 'shape factor' being eliminated. These derived moment-curvature relationships are also applied to determine column end rotations and mid-height deflections.

Two sizes of WF shapes are considered, (8WF31, 4WF13) and in the experimental studies, tests were carried out on as-delivered WF structural sections.

### II. Introduction

When extending the methods of analysis used in engineering mechanics to include the case of elastic-plastic bending, the relation between applied moments, axial thrust and resulting curvature for the case where stresses exceed the elastic limit is basic in importance, since it is the integrated effect of this curvature that determines deflections and rotations. The value of moment-deflection data is primarily in that it allows the determination of true maximum loads and the deflection at those loads. Moment-rotation data is also valuable since it enables one to evaluate performance relating to energy absorption. Further, it indicates the amount of rotation that a member may sustain at near-maximum moments.

For flexure in the elastic range the curvature,  $\phi$ , is given by

$$\phi = M/EI \quad (1)$$

where

$\phi$  = curvature,

$M$  = bending moment at the section in question,

$E$  = Young's modulus of elasticity, and

$I$  = moment of inertia of cross-section about axis perpendicular to plane of applied moments.

Equation (1) can be extended (neglecting certain higher order terms) in the form of the differential equation

\*Research Instructor, Fritz Engineering Laboratory, Lehigh University.

\*\*Formerly Research Assistant, Fritz Engineering Laboratory, at present, Research Engineer, David Taylor Model Basin.

\*\*\*Assistant Director, Fritz Engineering Laboratory, Lehigh University.

$$\frac{d^2y}{dx^2} = \frac{M}{EI} \quad (2)$$

By direct integration, Equation (2) defines all the various load-deformation relations.

On the other hand, above the elastic limit such ease of solution does not exist, since stress is no longer a linear function of strain and, therefore,  $\phi$  does not vary linearly with  $M$ . The problem of determining  $M-\phi$  relations in the plastic range has been solved for the condition of pure bending.<sup>10</sup> Since for that problem the neutral axis of strain coincides with the geometrical center of the section, relatively simple expressions were developed relating  $M$  and  $\phi$ . If, however, axial load is applied in addition to the imposed moment, such a strain condition no longer exists.

### 1. Influence of Axial Thrust

The determination of  $M-\phi$  curves including the effect of axial load has been developed by Timoshenko for the case of rectangular sections.\* For the case of WF shapes, discontinuities of the cross-section make direct computation troublesome, and in the next section of this report a 'point-by-point' method of computing  $M-\phi$  curves for rolled shapes is presented. It is similar to the method used earlier for the pure bending case,<sup>10</sup> but includes also the influence of axial thrust.

An important assumption made in this derivation is that the Bernoulli-Navier hypothesis (bending strain is proportional to the distance from the neutral axis) can be extended to include the case of plastic deformations.\*\* Using this hypothesis, together with assumptions with regard to properties of the material in question, this report outlines and illustrates a method whereby a relation between axial load, bending moment and curvature can be obtained even though stresses exceed the elastic limit.

The curvature,  $\phi$ , is a function of the strain developed at a section; the moment,  $M$ , and the axial thrust,  $P$ , are functions of the resultant stress. Fig. 1. Then,

$$P = \int_A \sigma dA \quad (3)$$

$$M = \int_A \sigma \cdot Y \cdot dA \quad (4)$$

$$\phi = \frac{\epsilon_1 - \epsilon_2}{d} \quad (5)$$

For the case of elastic strains illustrated in Fig. 1 (that is, when  $\epsilon_1 < \epsilon_y$  and  $\epsilon_2 < \epsilon_y$ ) the distribution of strain and distribution of stress are

\* Pages 51-54, Ref. (12)

\*\* Actually for steel members this is an idealization. As has been described in previous work (16), it is only required that in the elastic range, the strain be proportional to the distance from the neutral axis, and in the plastic range, that the stress be equal to the lower yield-point stress. Thus the curvature at any section is a function of the part which remains elastic. This is further discussed in Section III of this report.

If the strain-hardening range is considered, it is once again necessary to make an assumption with regard to strain distribution in the inelastic range. But strain-hardening has not been considered in this paper.

similar,  $\sigma_1$  being equal to  $E\epsilon_1$ , etc. When yielding occurs, however, this linear relation no longer holds; instead, there results a stress distribution composed of segments of various straight lines or curves depending on the stress-strain properties of the material in question.

In the analysis the idealized stress-strain diagram of Fig. 2 is assumed. This curve closely approximates the experimental stress-strain diagram of mild structural steel in the elastic and plastic ranges but strain hardening is neglected. Figure 3 is typical of the resultant stress and strain distribution curves when strains exceed the elastic limit. The stress is equal to the yield-point value when  $\epsilon > \epsilon_y$ . As would be expected, the moment corresponding to a given value of  $\phi$  would be less than that predicted using the straight-line relation of the elastic solution. However, by assuming a given stress pattern, it is possible to compute directly the corresponding value of  $\phi$ ; likewise,  $P$  and  $M$  may be determined. This may be done for various stress patterns and a curve plotted relating the three variables,  $P$ ,  $M$ , and  $\phi$ .\*

## 2. Residual Stresses

The behavior of structural members may be modified considerably by the presence of residual ('locked-in') stresses. A short review of their nature and influence is now presented.

Residual stresses are of two basic types: those due to differential cooling of the member during and after the rolling process, and those due to cold bending of the specimen while being straightened or during fabrication.

### Cooling Residual Stress

When the ingot is originally placed in the rolling mill, the temperature is nearly constant throughout the material. However, as it travels through the various rolls (each reducing the thickness of the different parts of the section), and later on the cooling bed, a differential in temperature develops. As a result of this differential and the subsequent plastic deformation of different parts of the cross-section at high temperature, the parts that cool the fastest are usually found to be in residual compression while the slower cooling portions indicate tensile residuals.

For a flat plate, the resulting stress distribution pattern after thermal equilibrium might be of the form shown in Fig. 4. Extending this reasoning to a rolled WF shape, the cooling residual stress pattern might be similar to that shown in Fig. 5. The mechanism, by which these residual stresses are formed has been described in several references.<sup>2,15</sup> The influence of cooling residual stresses on axially-loaded specimens has been described in a recent paper.<sup>6</sup>

The existence of such initial internal cooling stresses in 'as-rolled' steel members is demonstrated in several common shop practices. One is that of cutting a WF section along the center of the web to produce two T sections. As the cut progresses from one end of the beam toward the other, the individual T's deform--curving away from or toward each other, depending upon the distribution of residual stresses.

\* For the rectangular section it is not necessary to resort to graphical representation of the inter-relation between Equations (3), (4) and (5) since analytic expressions connecting these three variables are readily available. (See, for example, equations (42) and (47), page 37 and 39 of reference 4 or reference 13, page ).

As a basis for making an assumption with regard to the magnitude and distribution of residual stress, Fig. 6 shows a typical plot of measured residuals in the flanges and web for one of the sections considered in this investigation. The experimental points could be approximated either by parabolas or by straight lines. The latter has been chosen to facilitate computations and current work shows that this is a reasonable approximation for the shape studied.<sup>6</sup>

As re-plotted in Fig. 7, across each flange it is assumed that residual stress decreases linearly from a maximum compressive stress,  $\sigma_{rc}$ , at the flange edge to a tensile residual stress,  $\sigma_{rt}$ , at the web junction.

Furthermore, it is assumed that this tensile stress is constant across the web. It is required that  $\sigma_{rc}$  and  $\sigma_{rt}$  be chosen in such proportion that static equilibrium of the cross-section is maintained. This condition is assured if,

$$\frac{\sigma_{rt}}{\sigma_{rc}} = \frac{bt}{bt + w(d-2t)} = \frac{R_t}{R_c} \quad (5.1)$$

where

$b$  = Flange width

$t$  = Flange thickness

$w$  = Web thickness

$d$  = Section depth

$$R_t = \sigma_{rt}/\sigma_y$$

$$R_c = \sigma_{rc}/\sigma_y$$

#### Residual Stresses Due to Cold Bending

After the member passes through the last rolling mill and is cut into lengths suitable for handling, it is placed on the cooling bed. During cooling, the member tends to deform due to uneven support and other causes and, when cold, is no longer straight. Therefore, to obtain a straight finished product, each member must be cold bent. The conventional straightening method is to place the member in a 'gag' and plastically deform the curved part in the opposite direction to the original curvature. This 'gag' is diagrammatically shown in Fig. 8.

A member enters the 'gag' bent as shown by the solid line in Fig. 8. By applying a load, it is forced to the position indicated by the dashed lines. If on release of this load, the member is to have the straight form shown by the dash-dot position, a certain amount of yielding must take place to enable the 'permanent-set' to compensate for the original curvature. Since yielding has taken place, the strains in certain of the fibers have exceeded the elastic limit of the material and will, therefore, not return to their original positions on removal of the load. The balancing of these strains across the section produces cold-bending residual strains. Progress Report No. 5<sup>15</sup> contains a discussion of the magnitude and distribution of residual stresses formed as a result of cold-bending. Fig. 9 is typical of a 'cold bend' residual stress pattern for rectangular members (WF sections deformed about their weak axis).

Since plastic deformation is localized at points of load-application in the 'gag', it would appear that cold-bending residual stresses are also local in nature. At any rate, it is considered that these initial stresses do not have as pronounced an effect on column behavior as do cooling stresses which are

distributed rather uniformly along the length of the member. Therefore, detailed consideration of the influence of cold-bending residual stresses will not be made, emphasis being directed toward the cooling type of initial 'locked-in' stresses.

### 3. Stress Distribution Beyond the Elastic Limit

While the determination of stress-distribution and resulting moments and loads from an assumed yield condition is straight-forward for members without residual stress, the superposition of load-carrying strains and residual strains requires special attention for members that do contain residuals.

Consider the rectangular section of Fig. 10a which contains a certain residual strain (and stress) pattern. To this pattern of initial strain superimpose the strain pattern of an externally applied bending moment and thrust (defined by the applied strain pattern of Fig. 10b). If the total strains resulting from this superposition (as shown at the top of Fig. 10c) are within the elastic limit, the applied stress and applied strain patterns are similar across the entire section. Since  $\phi$  is a function of strain whereas  $M$  is a function of stress, it is clear that Equation 1 is applicable to this bending problem. When the combined strains exceed the elastic limit (Fig. 11c at top)  $\phi$  is no longer a linear function of  $M$ . Similarity between stress-and strain-distribution exists only for those regions in which the combined strains are less than the yield point (shown as  $d-y_{cc}$  in Fig. 11b). The resulting stress pattern (Fig. 11c) is determined directly from the strain pattern above. The applied stress pattern (Fig. 11b) is obtained by subtracting the initial residual stress pattern from the 'resulting stress pattern'. (This description is applicable to a WF column bent about the weak axis. . . so long as the web is neglected.)

Extending this reasoning to the case of flexure of a WF shape bent about its strong axis, the result of addition of residual and load-carrying strains is illustrated in Fig. 12. On the basis that plane sections before bending remain plane after bending, the applied stress patterns shown in Fig. 12 may be determined by the subtraction process just described. Under the applied moment and axial load shown diagrammatically, the stress-distribution for Case 1 is at the instant of first yielding of the compression flange. In Case 2, this flange is partially plastic and the tension flange has just reached the residual yield stress. When the compression flange is completely plastic (Case 3), the tension flange is still partially plastic. In Case 4, the member is completely plastic.\*

Similarly, for the cold-bending type of residual stress (cold bending assumed to have been about the weak axis of the section), 'stress addition' is shown in Fig. 13. Again, linear superposition of strains is assumed.

It is the purpose of this report to present a method for computing the moment-curvature relationship for WF columns, bent about either axis, and in the presence of axial thrust. It will also be shown how the presence of residual stress modifies the  $M-\phi$  relationship. Correlation with tests will be shown and the results will be used to predict the strength of as-delivered columns loaded with equal eccentricities. In the theory, the possibility of local and lateral-torsional instability is not considered.

\* P-M relationship is as described in Progress Report No.6<sup>(9)</sup>

### III. M- $\phi$ Relationship

#### 1. Members without Residual Stress

When a member is loaded within the elastic range by combined bending and thrust, stress and strain diagrams similar to those shown in Fig. 14 result. Since the strains are small in comparison to the depth of the section,

$$\phi = \frac{1 - \epsilon_2}{d} = \epsilon \frac{\sigma_1 - \sigma_2}{Ed} \quad (5a)$$

For members loaded beyond the elastic limit (Fig. 15)

$$\phi = \frac{1 - \epsilon_2}{d} = \epsilon \frac{\epsilon_y - \epsilon_2}{(d - t_{cc})} \quad (5b)$$

or

$$\phi = \frac{\sigma_y - \sigma_2}{E(d - y_{cc})}$$

It is thus possible to compute  $\phi$  directly from a stress diagram by considering only that part of the section which remains elastic.

From a stress diagram, it is also possible to determine both the moment acting on the section and the applied thrust.<sup>12</sup> By using Equations (3), (4) and (5b) it is then possible to determine M, P and  $\phi$  for any given stress distribution.

As loads are increased under a given loading condition, it is likely that successive stress-distributions will be similar to those shown in Fig. 16. Yielding will first occur at the extreme fiber on the compression side of the specimen. As the loading is increased, yielding will penetrate through the flange on the compression side. Eventually, yielding occurs on the tension side--Sketch (c)--and the full plastic condition is typified by Sketch (d).

For ease of computation certain flexure conditions are assumed, and a typical set of these is illustrated in Fig. 17. From the equilibrium conditions, values of P and M may be determined for each assumed value of  $\phi$ . This makes it possible to plot curves of P vs  $\phi$  and M vs  $\phi$  for any given value of yield penetration on the compression side. One such set of curves is shown in Fig. 18 for an 8WF31 section where yielding was assumed to have penetrated to a depth of 1/4d from one side. (It is Case (c) of Fig. 17.) These curves have been made non-dimensional by plotting  $P/P_y$  vs  $\phi/\phi_y$  and  $M/M_y$  vs  $\phi/\phi_y$ . For all points plotted, the corresponding stress distribution diagrams have been shown.

Curves similar to Fig. 18 have been computed for each of these assumed values of yield penetration for the 8WF31 section and are presented in Fig. 19. Since the straight-line portion of each of these curves is that corresponding to an elastic stress condition on the tension (convex) side of the section, only the limiting cases where  $\sigma_a$  = yield point stress in compression and tension need be investigated to define that part of each curve. The limit of this range has been shown as a dash-dot line.

The method of using these 'auxiliary curves' (Fig. 19) is to select a value of  $P/P_y$  for which a M- $\phi$  curve is desired. For example  $P = 0.2P_y$ . With this value of  $P/P_y$  draw a horizontal line cutting the various auxiliary P- $\phi$  curves. At these points of intersection, project verticals until they intersect the corresponding M- $\phi$  auxiliary diagrams. Connecting these points gives

the desired  $M - \phi$  curve including the effect of an axial thrust of  $0.2P_y$ . (This process is indicated in Fig. 19 by dashed lines.) Fig. 20 is the desired curve with the auxiliary construction lines removed.

The curved portions of Fig. 19 have been plotted to a larger scale in Fig. 21 to facilitate greater accuracy in this graphical method. Here  $M - \phi$  curves for several different values of  $P/P_y$  have been shown (dashed lines).

The influence of varying axial load for a range of  $P/P_y$  is illustrated in Fig. 22.  $M - \phi$  curves have been plotted here for various values of  $P/P_y$  ranging from 0 to 0.8. As indicated by the dashed line, only when  $P$  is relatively small will the tension flange be plastic. For the range in which it remains elastic, only the straight-line portion of each auxiliary curve need be considered to obtain the desired  $M - \phi$  curve.

Table 1 contains equations necessary for plotting critical points on the 'Auxiliary curves' (Fig. 19 or 21). It will be recognized that the computation is time-consuming and tabular solution appropriate.

No tests using annealed material were conducted as part of this investigation and consequently comparison between the theory and test is not made here. However control tests on axially-loaded columns were carried out on the 8WF31 material as part of another study<sup>6</sup>.

## 2. Members Containing Residual Stress

By a process analogous to that just described, expressions for  $P$ ,  $M$  and  $\phi$  may be developed for assumed 'yield conditions' for sections containing residual stresses. (See Fig. 12 for flexure about the strong axis, Fig. 11 for weak axis bending). The equations for flexure about the strong axis are shown in Table 2 and those for flexure about the weak axis are given in Table 3\*. In these equations,

$$R_a = \sigma_a / \sigma_y$$

$$R_c = \sigma_{rc} / \sigma_y$$

$$R_t = \sigma_{rt} / \sigma_y$$

$$\alpha = y_{cc} / d$$

$$\beta = y_{tt} / d$$

The equations summarized in Table 2 reduce to those shown in Table 1 for annealed material when the residual stress is zero ( $R_c = R_t = 0$ ).

Auxiliary  $P - \phi$  and  $M - \phi$  curves are shown in Fig. 23 for one 'alpha' condition ( $\alpha = 0.4$  indicates that yielding has penetrated to four-tenths the depth of the member). The assumed residual stress function ( $R_c = 0.3$ ) is consistent with actual residual stress measurements. The Figure also shows the auxiliary curves for material free from residual stress. These curves have also been made non-dimensional by plotting  $P/P_y$  - vs-  $\phi/\phi_y$  and  $M/M_y$  - vs-  $\phi/\phi_y$ . The portions which are cross-hatched correspond to regions covered by the equations of Tables 1 & 2. Where shading is missing, the member has partially yielded in the tension flange and the equations for this short region are not presented.

This method of assuming a penetration of yielding on the compression side of the section and then determining curves of  $P$  - vs-  $\phi$  and  $M$  - vs-  $\phi$  can be carried out for any value of yield penetration. Six different values were

\* In the derivation of these weak axis equations the web was neglected and the section was considered as two equivalent rectangles. In reality then these expressions of  $M$ ,  $P$  and  $\phi$  apply strictly to the rectangular section.

assumed to obtain the curves presented in this report. For each, a set of curves similar to those of Fig. 23 was plotted preparatory to plotting the  $M-\phi$  curves. The latter are obtained for a given axial load by drawing a horizontal line cutting the various auxiliary  $P-\phi$  curves at the assumed axial load value ( $P/P_y = 0.4$  has been chosen for illustration). At these points of intersection, project verticals until they intersect the corresponding  $M-\phi$  auxiliary diagrams (circled in Fig. 23). Plotting the values obtained from each of the separate 'auxiliary curves' and connecting the corresponding points gives the desired curves. These are plotted in Fig. 24, the points obtained from Fig. 23 being circled for illustration.

Typical  $M-\phi$  curves for flexure about strong and weak axes for the 8WF31 section are shown in Figs. 25 and 26, respectively. In each of these figures, solutions neglecting the influence of residual stress are shown by solid lines whereas those including this variable are indicated by dashed lines. As expected, the influence of residual stress on  $M-\phi$  curves is more pronounced for flexure about the weak axis.

### 3. Measurements

In Figures 27-31 are plotted the  $M-\phi$  relationships obtained in the course of testing sixteen different columns and Table 4 summarizes the pertinent loading information for each of the tests reported. It also indicates for each specimen the observed mode of failure. All specimens were tested in the as-delivered condition and two sizes were used (8WF31 and 4WF13) in a range of  $L/r$  from 21 to 111. Details of test apparatus and procedure are described in Ref. 3 and Ref. 9 summarized the behavior of the specimens tested.

The curvature,  $\phi$ , at any section is a measure of the variation in strain differences across the section. SR-4 strain gages were placed symmetrically about the centerline of the section at a known distance from one another, this distance being such that  $\phi$ -measurements could be made relatively far into the inelastic range. They were placed as close as practicable to the section at which maximum moment was expected.

Moment values at ' $\phi$ -sections' were determined as the sum of applied end moments and the product of applied axial thrust and measured deflections.

In Figs. 27 through 31 both experimental and analytical  $M-\phi$  curves are presented.\* With each set of curves is shown the loading condition with the column in its deflected configuration. The shaded arrows denote the location of the section at which  $\phi$  was measured. The other auxiliary sketch is an interaction curve<sup>9</sup> which shows the maximum values of axial thrust and end bending moment at collapse as well as the path followed in obtaining that loading.

The theoretical  $M-\phi$  solutions neglecting residual stress are shown by dashed lines. For an assumed flange tip residual stress equal to three-tenths of the yield stress (i.e.,  $R_c = 0.3$ ), the theoretical curve is shown by a dash-dot line. The experimental curves are shown solid. Initial yield as determined by flaking of the mill scale coated with whitewash is shown for each test by the open arrows.

In the figures the symbol 'LA' denotes lateral buckling as observed with the aid of dial gages and SR-4 gages; the symbol 'L' indicates observed local buckling. Point 'LA' was well defined by the measurements made. (The mode

\* The material properties for the two sections investigated are tabulated in Table 5.

of failure shown in Table 4 is an effort to show how the column finally collapsed). In each case, lateral buckling occurred at a moment higher than the first observed inelastic action, but the onset of lateral buckling is in most cases not the maximum observed moment. Rather, it is a point at which deformations commence to increase at a more rapid rate. For most of the specimens, the test results are in fair agreement with the theory up to the point at which lateral-torsional buckling was observed.

Referring to Fig. 28, the location of the open arrows suggests that the residual stress level was about the same in each of these specimens ( $R_c = 0.26$ ). This is interesting because two different rollings from the same ingot were involved. Further, since lateral buckling ('LA') was observed for each of these condition 'c' tests at about the same moment and since the slenderness ratios are different ( $L/r$  varies from 27 to 55), inelastic lateral buckling in this range appears to be a function of maximum moment and is not much affected by the length.

The behavior of T-13 (Fig. 29) is different from the rest of the eight-in. specimens, the curve closely approaching that for a member without residual stress. A possible explanation is that the member might have been cold-bent in the region at which  $\phi$  was measured thus wiping out the cooling residual stresses.

In Fig. 31, showing the results of tests on four-in. members, the open arrows indicate that this material had a lower level of residual stress than did the eight-in. material. (The average value for all 4-in. specimens tested was  $R_c = 0.1$  whereas that for the 8-in. specimens was  $R_c = 0.24$ ).

Specimens T-3 (Fig. 27) and T-21 (Fig. 30) were identical except for the size of member. The measured  $M-\phi$  curves are also similar, deviating markedly from the theoretical curve. This seems to be characteristic behavior when a relatively greater axial load is applied to the member. Also owing to the fact that the column is effectively restrained by the condition 'b' loading, lateral buckling is not observed until a considerable amount of plastic deformation has occurred. Incidentally, the reduction in strength of the theoretical curves to T-21 below those of T-17 and T-20 indicates the influence of axial thrust summarized earlier in Fig. 25.

Good correlation between theory and test is observed in T-7 and T-9 (Fig. 29) for 4-in. material even though two different rollings from the same ingot are involved.

In Fig. 32 are plotted  $M-\phi$  curves for several different tests. It is seen that the experimental results are consistent.

Examining the individual curves for tests 12, 14, 16, and 19 (Figs. 27, 28) the  $M-\phi$  behavior is relatively consistent for these 8WF31 specimens below the point at which twisting of the specimen was noted. It would not be expected that the theory would apply beyond the point at which buckling failure occurred. However, even prior to lateral-torsional buckling the curves did not correspond exactly to theory. Several reasons for this discrepancy are:

- (a) The assumed residual stress pattern (straight-line variation) is an idealization. A variation in magnitude of residual stress also will affect the  $M-\phi$  curve.
- (b) It was assumed that yielding progressed uniformly to known, given depths ( $y_{cc}$  and  $y_{tt}$ ); however, steel does not behave in this manner, certain parts yielding more and others yielding less than supposed. This problem has been extensively discussed in Progress Report No. 5<sup>15</sup>, and Fig. 33 selected from that report suggests that curvature for a given moment would be greater than predicted by the theory described earlier in this paper.

#### IV. Column Strength

The results obtained in the previous section will be applied to a consideration of the eccentrically loaded member shown in Fig. 34. This single curvature loading condition is essentially the same as loading condition 'c' (Table 4). The member is assumed to be initially straight, of uniform cross-section and free from accidental eccentricities. For WF shapes it is of interest to determine the following:

- (a) the ultimate strength of the eccentric column
- (b) the load-deflection relationship for columns with equal eccentricities
- (c) the end-rotation of columns in the plastic range.

Knowledge of the  $M-\phi$  relationship makes possible a solution to these problems--including also the influence of residual stresses.

The strength of the eccentrically-loaded column has been considered by Bleich, who reviewed the work done up to that time.<sup>4</sup> As he pointed out, a determination of true column strength depends on a knowledge of the load-deflection relationship (Problem 'b', above). End rotations (problem 'c') are possibly of academic interest for columns loaded with equal eccentricities. Such members collapse quickly after reaching the maximum load. They have little 'rotation capacity', i.e., the ability to deform through considerable angle changes at near-maximum loads. On the other hand, columns bent in double curvature may show considerable 'rotation capacity', and indeed this is required if structural members are to meet the assumption implicit in plastic analysis and design.\*

##### 1. Load-Deflection Relationship

The difference between the elastic and the plastic load-deflection relationship is shown in Fig. 36. The equation of the elastic curve is

$$\frac{\Delta}{e} = \frac{1 - \cos u}{\cos u} \quad (6)$$

where

$u = kL/2$ ,  $e$  = eccentricity of load,  $\Delta$  = centerline

deflection, and  $k = \sqrt{P/EI}$ .

Even with large eccentricities, the maximum elastic strength approaches the Euler buckling load. However, as the load increases, the stress in the outermost fibers at the center section of the column increases at a faster rate due to the bending moment which is increasing as the product of  $P$  and the quantity  $(\Delta + e)$ . See Fig. 34. Therefore, columns of the proportions used in engineering structures start to yield, say at some point 'a' in Fig. 36. As the compressive force,  $P$ , is increased beyond this initial yield value, plastic flow spreads from the edges towards the center of the section and along the bar thereby reducing its flexural rigidity. Consequently, the deflection,  $y$ , (and hence the moment of the external forces) increases at a higher rate than for the elastic case. Finally a point is reached at which further increase in load is impossible and collapse occurs. This maximum load would correspond to point 'b', the portion 'b-c' representing the inelastic, unstable load-deflection relationship.

The load deflection curve is determined by integration of  $\phi$ -values. However,  $\phi$  is dependent upon the bending moment which in turn is dependent

\* This is discussed in several papers, most recently in Ref. 8. Column end rotations have been examined in a recent unpublished report, 'Moment-Rotation Characteristics of Beam-Columns', by R.L. Ketter and L.S. Beedle, Progress Report R, Fritz Laboratory Report 205A.11, November, 1952.

itself upon the deflection. A numerical integration procedure<sup>11</sup> is suitable in problems of this type. A deflected shape is assumed and moments are computed.  $\phi$ -values are obtained (Section III) and these are integrated to obtain a new deflected shape. If the assumed curve is correct, the deflection values obtained will be identical with the former. This method was applied to the members studied in the program and Fig. 35 shows typical resulting curves. The solid curve is the experimental result and the theoretical curves using the numerical method are shown by dot-dash lines for zero residual stress and for residuals estimated at three-tenths of yield-point stress.

Agreement is reasonable up to the point at which the member starts to twist.

Even though the exact deflected configuration is that which results in the lowest potential energy of the system, the magnitude of the critical load is relatively insensitive to changes in the assumed deflection curve providing the deflection patterns conform to the geometric boundary conditions of the member. Bleich<sup>4</sup> describes the use of an assumed sine curve by Jezek and an assumed partial cosine curve by Osgood and Westergaard. These two assumptions have also been used in the following paragraph toward the determination of column buckling loads in the inelastic range.

Assuming that the column bends in a sine curve,

$$y = \Delta \sin \frac{\pi x}{L}$$

The section at mid-height is subjected to the greatest deformation, and  $\phi$  at this section is

$$\phi = \left. \frac{d^2y}{dx^2} \right|_{x=\frac{L}{2}} = \frac{\pi^2}{\frac{L^2}{4}} = \frac{4\pi^2}{L^2} \Delta \quad (7)$$

The moment at this same section for the eccentrically loaded column is given by

$$M = P (\Delta + e) \quad (8)$$

and for the condition- 'c' -loaded column by

$$M = M_0 + P \Delta \quad (9)$$

From Eq's. (7), (8) or (9) and the  $M-\phi$  plot for the section in question, load-deformation curves may be obtained. A typical resulting curve is shown in Fig. 35 by dotted lines for the two material conditions (annealed and as-delivered). The predicted maximum end moment agrees with the numerical method within one percent.

Referring to Fig. 34, the deflection expressions for a partial cosine curve is given by

$$y = (\Delta + e) \cos \frac{\pi x}{L+a} \quad (10)$$

Then, by using the first two terms of a cosine series,

$$\phi = -\frac{8.0}{L^2} \cdot \Delta \quad (11)$$

In this case the resulting end-moment vs deflection curve coincides almost exactly with the numerical integration curve of Fig. 35 and has therefore not been shown.

Reviewing the detailed steps which were followed in obtaining these approximate load-deflection curves;

- (a) Assume a center line deflection,  $\Delta$ .
- (b) Using either equation (7) or (11), compute  $\phi$ .

- (c) Enter the appropriate  $M-\phi$  curves with the value of  $\phi/\phi_y$  and read off the corresponding  $M/M_y$  ratio.
- (d) Compute  $M_o$  or  $P$  from either equation (8) or (9).

## 2. Strength of Eccentric Columns

The ordinary column curve presents strength as a function of slenderness ratio,  $L/r$ . By using the sine curve assumption and the  $M-\phi$  curves of Fig. 25 and 26, column curves are obtained as presented in Fig. 37 (strong axis bending) and Fig. 38 (weak axis bending). Data is shown on a non-dimensional basis, the maximum load being divided by  $P_y$ , determined from the product of yield-point stress and cross-sectional area. The curves show the influence of end eccentricity and of residual stresses. Three curves are shown for each eccentricity ratio ( $ec/r^2$ ): the maximum strength of annealed members, the maximum strength of as-delivered columns containing residual stresses and the initial yield (secant) solution. The shaded portion at each eccentricity shows the influence of residual stress on collapse strength. Curves of allowable load according to the A.A.S.H.O. Specification<sup>1</sup> are also shown.

The curves show that the secant solution is on the unsafe side for intermediate length columns with small eccentricities and that it is too conservative for short members, the latter being particularly true for large eccentricities. For small eccentricities, columns will collapse at loads considerably less than predicted by the initial yield condition. At zero eccentricity the considerable reduction due to residual stress has been confirmed by tests and is reported upon separately.<sup>6</sup>

Fig. 39 is a cross-curve of Fig. 37 (strong axis) at  $L/r=55$ . In addition to the various theoretical solutions the results of three tests are shown. The collapse strength for each of these test members is less than the theoretical solution that includes the influence of residual stress. This is due, in part at least, to flexural-torsional buckling of columns bent about the major axis, the mode of failure observed for each of these tests.

The 'collapse' curves of Fig. 37, 38 and 39 are based on the assumption that the section deforms only in the plane of the applied moments and that during this deformation it maintains its original cross-sectional form. While this is satisfactory for weak axis bending, lateral-torsional buckling occurs when flexure is forced about the strong axis of the section. A solution to this problem is to be sought in the program currently underway at Lehigh.

An opportunity to compare the theory with the results of tests on annealed columns is afforded by experiments carried out recently at Cornell<sup>14</sup>. In that investigation columns were allowed to bend about the weak axis. Fig. 41 shows the comparison between the theoretical solution outlined above and the results of experiment (circles). The theoretical curve is obtained by making a cross-curve of Fig. 38 at an  $L/r$  of 50, the I-shape being approximated by two equivalent rectangles. It is seen that the agreement is good. As-delivered specimens were also tested, but since the level of residual stress is not known, the corresponding test points and the theoretical curve have not been plotted, although a rough approximation to a possible residual stress pattern yields a fair correlation between test and theory.

## 3. Moment-Rotation Relationship

Typical end-moment vs end-rotation curves are shown in Fig. 40. The theoretical curves obtained by the method of numerical integration are shown by dashed lines, the test result shown by the solid line. For the theory that

takes into account residual stresses, and in the region prior to twisting of the cross-section, agreement with test is excellent.

## V. Discussion and Summary

### 1. M- $\phi$ Relationship with Axial Thrust Present

A method has been presented for determining the influence of axial load on the moment-curvature relationship in the plastic range. Simultaneous thrust-, moment-, and curvature-values are determined (Table 1) for different yield conditions, and from these are constructed 'auxiliary curves' (Fig. 19). Once these auxiliary curves are plotted for a particular wide-flange shape, the M- $\phi$  relation may be obtained conveniently for any desired value of axial load (Fig. 22).

A significant reduction in moment-carrying capacity at a given cross-section is to be expected in the presence of axial thrust. (Fig. 22).

Previous solutions were limited to rectangular shapes. This graphical method extends the solution to Wide-flange and other symmetrical shapes. Since all rolled shapes contain some residuals, the solution has practical application in that it may be extended to members containing such 'locked-in' stresses.

### 2. Influence of Residual Stress

The above method may be applied to members containing residual stresses after a distribution pattern for such stresses has been assumed (Fig. 6, 7). For flexure about the strong and weak axis, equations are developed (Tables 2 and 3) for the construction of auxiliary curves (Fig. 23) from which M- $\phi$  curves can be obtained by graphical construction (Figs. 25, 26).

For a given axial thrust, residual stresses increase the deformation in such a way that it appears as though the moment strength were reduced. If straining can be continued sufficiently without column buckling occurring, the effect of residual stress is wiped out and the strength reaches the predicted value (Fig. 25). Tests show that column collapse may occur in the region in which residual stress is of influence (Fig. 28), and this is discussed further in the next section.

The influence of residual stress is more pronounced for members bent about the weak axis than for those bent about the strong axis (Fig. 26 compared with Fig. 25).

Test results in general confirm the theory up to the point at which lateral deformation commences for members bent about the strong axis. 'Weak-axis' experimental data will be available later in the program which is currently underway.

### 3. Column Behavior

Application of the M- $\phi$  data derived in this report to compute load-deflection curves for eccentrically-loaded columns (by numerical integration) gives reasonable correlation with test results up to the point of twisting (Fig. 35). A nearly identical solution is obtained by assuming a partial cosine curve.

Excellent correlation between theory and test (up to the point of twisting) is obtained for the relationship of end bending moment to end rotation of the column (Fig. 40).

The ultimate strength of eccentrically loaded columns may be determined by the maximum point of a load-deflection curve. The results obtained using

such a procedure are summarized in the column curves of Figs. 37 and 38 and show the maximum strength of annealed members, of members containing residuals, and the yield stress (secant) solution. The reduction in collapse strength due to residual stress (shaded) at  $L/r = 85$  ranges from 22% for  $ec/r^2 = 0$  to about 4% for each  $ec/r^2 = 1.0$  for the strong axis. Similarly columns which collapse due to bending about the weak axis suffer theoretical strength reductions of 26% at zero eccentricity to 6% at  $ec/r^2 = 1.0$ .

The initial yield solution (secant) is generally on the unsafe side for intermediate length members with small eccentricities, and is too conservative for short members.

Fair correlation between theory and test is established in Fig. 39 for a few columns bent about the strong axis and which eventually collapsed by lateral-torsional buckling.

Final failure for all members tested in the entire program was due either to lateral-torsional buckling or to local buckling (Table 4). However all of the theoretical curves derived and presented herein assume that failure is due to simple column bending. A consideration of test results (see Fig. 40, for example) suggests that the influence of residual stress might be more than the initiation of yielding at low loads with the subsequent loss in buckling strength shown in the theoretical curves. This early yielding due to residual stresses may aggravate the tendency toward lateral and/or local buckling; further studies are being made on the problem of inelastic instability.

A considerable amount of computation and plotting is involved in obtaining these results; simplified expressions are required which will sufficiently describe the behavior of these columns. Work has been started to apply the results to columns under different loading conditions and with end restraints. The column strengths here reported represent a 'worst case'. Higher strengths will be expected for other loading conditions and end restraints.<sup>14</sup>

Whatever column analysis is made, the basic relationship is that of moment to curvature. The results presented here are dependent upon an assumed magnitude and distribution of residual stress. The assumption seems reasonable, in the light of measurements that have been made up to this time. Eventually, when more data is collected, current design rules may be re-examined toward providing more economical structures consistent with adequate safety.

## VI. Acknowledgements

The authors wish to acknowledge the contributions made toward the investigation by the work of Chien-Huo Chen, Jan M. Ruzek, and Donald L. McCullough. This work has been carried out as part of an investigation sponsored jointly by the Welding Research Council and the Navy Department with funds furnished by the following: American Institute of Steel Construction, American Iron and Steel Institute, Column Research Council (Advisory), Office of Naval Research (Contract No. 39303), Bureau of Ships and Bureau of Yards and Docks. The helpful criticisms of members of the Welding Research Council, Lehigh Project Sub-committee (T.R. Higgins, chairman), and the Column Research Council Research Committee D (N.M. Newark, chairman and N.J. Hoff, co-chairman) are sincerely appreciated. This program is being carried out in the Fritz Engineering Laboratory of which Professor William J. Eney is Director.

## VII. Nomenclature

<b>A</b>	= Area of cross-section
<b>b</b>	= Flange width
<b>d</b>	= Depth of WF section
<b>E</b>	= Young's modulus of elasticity
<b>M</b>	= Moment
<b>M<sub>o</sub></b>	= Moment applied at the end of a member
<b>M<sub>y</sub></b>	= Moment at which yield point is reached in flexure
<b>M<sub>yc</sub></b>	= Moment at which initial outer fiber yielding occurs when axial thrust is present
<b>P</b>	= Concentric axial thrust on a column
<b>P<sub>y</sub></b>	= Axial load corresponding to yield stress level over entire section
<b>R<sub>c</sub></b>	= Ratio of the maximum compressive residual stress, $\sigma_c$ , to the yield stress level, $\sigma_y$
<b>R<sub>t</sub></b>	= Ratio of the maximum tension residual stress $\sigma_t$ to the yield stress level, $\sigma_y$
<b>S</b>	= Section modulus
<b>t</b>	= Flange thickness
<b>w</b>	= Web thickness
<b>y<sub>cc</sub></b>	= Depth of yield penetration in compression
<b>y<sub>tt</sub></b>	= Depth of yield penetration in tension
<b>y<sub>ct</sub></b>	= Distance from yield penetration in compression to extreme fiber in tension
<b>Z</b>	= Plastic modulus
<b><math>\alpha</math></b>	= Ratio of the depth of yield penetration in compression to the total depth of the section (i.e., $\alpha = \frac{y_{cc}}{d}$ )
<b><math>\beta</math></b>	= Ratio of the depth of yield penetration in tension to the total depth of the section (i.e., $\beta = \frac{y_{tt}}{d}$ )
<b><math>\Delta</math></b>	= Centerline deflection of a beam-column loaded to produce single curvature
<b><math>\epsilon</math></b>	= Strain
<b><math>\epsilon_y</math></b>	= Strain corresponding to yield point stress
<b><math>\epsilon_{rc}</math></b>	= Maximum residual compressive strain
<b><math>\epsilon_{rt}</math></b>	= Maximum residual tensile strain
<b><math>\sigma</math></b>	= Normal stress
<b><math>\sigma_y</math></b>	= Lower yield point stress
<b><math>\sigma_{rc}</math></b>	= Maximum residual compressive stress
<b><math>\sigma_{rt}</math></b>	= Maximum residual tensile stress
<b><math>\sigma_a</math></b>	= Variable normal stress on tension side of specimen (positive when in tension)
<b><math>\phi</math></b>	= Curvature at a section
<b><math>\phi_y</math></b>	= Curvature corresponding to initial outer fiber yielding ( $P = 0$ )
<b><math>\theta_A</math></b>	= Column end rotation (at end A)

## VIII. References

1. American Association of State Highway Officials, 'Specification of Highway Bridges', American Association of State Highway Officials Washington, D.C., (1949)

2. American Welding Society, 'Welding Handbook', American Welding Society, New York, 3rd. Ed., (1950)
3. Beedle, Lynn S., Ready, Joseph A., and Johnston, Bruce G., 'Tests of Columns Under Combined Thrust and Moment', PROGRESS REPORT NO. 2, PROCEEDINGS OF THE SOCIETY FOR EXPERIMENTAL STRESS ANALYSIS - Vol. VIII, No. 1, 109 (1950)
4. Bleich, F., 'The Buckling Strength of Metal Structures', McGraw-Hill Book Company, New York, 1st. Ed., (1952)
5. Chwalla, E., 'Der Einfluss der Querschnittsform auf das Tragvermögen aussermittig gedruckter Baustahlstäbe', DER STAHLBAU, Vol. 8, p. 193, (1935)
6. Huber, Alfons W., and Beedle, Lynn S., 'Residual Stress and the Compressive Properties of Steel', Publication schedules in THE WELDING JOURNAL
7. Jezek, K., 'Die Tragfähigkeit des gleichmäßig querbelasteten Druckstabes aus ideal-plastischen Stahl', DER BAUTECHNIK, Vol. 5, p. 33, (1935)
8. Johnston, Bruce G., Yang, Ching Huan, and Beedle, Lynn S., 'An Evaluation of Plastic Analysis as Applied to Structural Design', PROGRESS REPORT NO. 8, THE WELDING JOURNAL, Research Supplement (1953)
9. Ketter, Robert L., Beedle, Lynn S., and Johnston, Bruce G., 'Column Strength Under Combined Bending and Thrust', PROGRESS REPORT NO. 6, THE WELDING JOURNAL 31(12), Research Supplement, 607-s to 622-s (1952)
10. Luxion, William W., and Johnston, Bruce G., 'Plastic Behavior of Wide Flange Beams', PROGRESS REPORT NO. 1, THE WELDING JOURNAL 27(11), Research Supplement, 538-s to 554-s (1948)
11. Newmark, N.M., 'Numerical Procedure for Computing Deflections Moments and Buckling Loads', TRANSACTIONS OF THE A.S.C.E., Vol. 108, p. 1161-1234, (1943)
12. Timoshenko, S., 'Theory of Elastic Stability', McGraw-Hill Book Company, New York, (1936)
13. Wastlund, George, and Bergstrom, Sven G., 'Buckling of Compressed Steel Members', TRANSACTIONS OF THE ROYAL INSTITUTE OF TECHNOLOGY, Stockholm, Sweden, (1949)
14. Winter, George, Fisher, G.P., and Bijlaard, P.P., 'Plastic Buckling of Eccentrically Loaded Elastically Restrained Columns', Publication scheduled in PROCEEDINGS, American Society of Civil Engineers, (1953)
15. Yang, Ching Huan, Beedle, Lynn S., and Johnston, Bruce G., 'Residual Stress and the Yield Strength of Steel Beams', PROGRESS REPORT NO. 5, THE WELDING JOURNAL 31(4), Research Supplement, 205-s to 229-s, (1952)
16. Yang, Ching Huan, 'The Plastic Behavior of Steel Beams', Ph.D. Dissertation, Lehigh University, January, (1951)

**TABLE I**  
**SUMMARY OF IMPORTANT EQUATIONS**  
**Strong Axis, WF Section Bending**  
**(Neglecting Residual Stresses)**

TOP FLANGE (Compression)	WEB	BOTTOM FLANGE (Tension)		$\sigma_y$	$\sigma_a = \frac{\sigma_a}{\sigma_y}$	$\alpha = \frac{y_{CC}}{d}$	$\beta = \frac{y_{fl}}{d}$	<b>CASE 3</b>
				$R_a = \frac{\sigma_a}{\sigma_y}$	$\alpha = \frac{y_{CC}}{d}$			<b>CASE 2</b>
LIMITS				$\frac{P}{\sigma_y} = (1-R) \left[ b(1-w) + \frac{(1+R_a)}{2d(1-\alpha)} \right]$	$\frac{P}{\sigma_y} = \frac{1}{d} \epsilon \alpha^{\frac{1}{2}} (1 - \frac{1}{2})$ $- 1/4 R_a \epsilon^2$	$\frac{1}{d} \epsilon \alpha^{\frac{1}{2}} (1 - \frac{1}{2})$ $- 1/4 R_a \epsilon^2$	$\frac{P}{\sigma_y} = w d (1 - \beta)$	
AXIAL THRUST				$\frac{P}{\sigma_y} = \frac{1-R_a}{2} [2w(1+w(d-2))]$				
MOMENT				$\frac{M}{\sigma_y} = \frac{1+R_a}{12d} [2b(3d^2-6d+4)^2] + w(d-2)^2$	$\frac{M}{\sigma_y} = \frac{(1+R_a)}{12d(1-\alpha)} \left[ w \left\{ d(1-\alpha - \frac{1}{d}) \right\}^2 \{ d(1-2\alpha) - 4 \} \right]$ $6d(1-\alpha)(d-1) - 3d^2 + 4^2$	$\frac{M}{\sigma_y} = b(1(d-1)) + \frac{w^2}{6} \left[ \frac{6}{(\beta - \frac{1}{d})(1-\beta - \frac{1}{d})} \right]$ $+ ((1-\alpha - \beta)(1+2\alpha - 4\beta))$		
CURVATURE				$\frac{\phi}{\phi_y} = \frac{1+R_a}{2(1-\alpha)}$			$\frac{\phi}{\phi_y} = \frac{1}{1-\alpha - \beta}$	

**TABLE 2**  
**SUMMARY OF IMPORTANT EQUATIONS**  
**Strong Axis, WF Section Bending**  
**(Including Residual Stresses)**

<p>TOP FLANGE (Compression)</p> <p>WEB</p> <p>BOTTOM FLANGE (Tension)</p>	<p>CASE 2</p> <p>CASE 3</p>	<p>CASE 3</p>
$R_g = \frac{\sigma_0}{\sigma_y}$ $\alpha = \frac{y_{cc}}{d}$	$R_g = \frac{\sigma_0}{\sigma_y}$ $\alpha = \frac{y_{cc}}{d}$	$\alpha = \frac{y_{cc}}{d}$ $\beta = \frac{y_{ff}}{d}$
$\frac{1}{d} \times \alpha = (1 - \frac{1}{d})$ $-(1 - R_c) \times R_g + \gamma(1 - R_t)$	$\frac{1}{d} \times \beta = \beta \times (1 - \alpha) \times 2 + \gamma c_e R_t$ $\frac{1}{d} = \alpha = (1 - \frac{1}{d})$	$\frac{P}{\sigma_y} = \frac{b}{2} \left[ 2 \cdot R_c + R_t - 2 R_g \left( \frac{d}{d-a} \right)^{1-a} R_t + R_g \right] + w \left[ (1 + R_t) \left( 1 - \frac{1}{d} \right) \right.$ $\left. - \frac{1}{2} (1 - \alpha - \frac{1}{d}) (1 - \frac{1}{d-a}) \right] - \frac{R_g}{2} (1 - \alpha - \frac{1}{d}) \times (1 - \frac{1}{d(1-\alpha)})$
$\frac{M}{\sigma_y} = \frac{b}{12} \left[ 3(a-1)(2 - R_c - R_t + 2R_g) - (3d - 4) \gamma \left( \frac{1+R_g+R_t}{1-\alpha} \right) \right]$ $+ \frac{wd}{12(1-\alpha)} \left[ (1 - \alpha) - \frac{1}{d} \right] \left[ -\frac{4}{d} + 2 \alpha (1 + R_g + R_t) (d(1-\alpha) - 1) \right]$	$\frac{M}{\sigma_y} = \frac{1}{6} [(d-1)(b-w) + \frac{wd^2}{6}] + \alpha + \beta - 2\alpha^2 + 2\alpha\beta - 2\beta^2$	$\frac{\phi}{\phi_y} = \frac{1 + R_g + R_t}{2(1-\alpha)}$
CURVATURE		$\frac{\phi}{\phi_y} = \frac{1}{(1-\alpha-\beta)}$

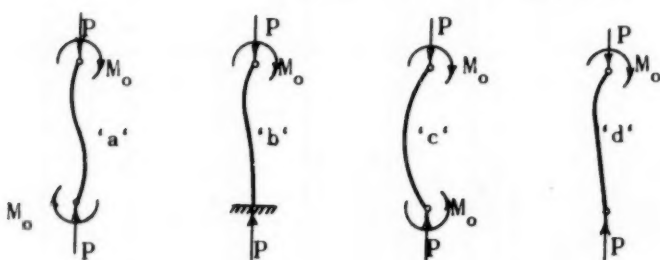
TABLE 3

**SUMMARY OF IMPORTANT EQUATIONS**  
**Welded Axis, WF Section Bending**  
**(Including Residual Stresses)**

<p><b>CASE 1</b></p> <p>LIMITS</p> $\frac{\sigma_y - \sigma_{yC}}{R_g} \leq \frac{a}{D}$ $-\left(1 - R_C\right) \leq R_g \left(1 + R_C\right)$ $R_g \leq \frac{R_C(a-1) + (a+1) + 2aR_t}{1-a}$ <p>* Condition for Pure Bending</p>	<p><b>CASE 2</b></p> <p>LIMITS</p> $0 \leq a \leq 1/2$ $\beta = R_t/2$ $\beta^2 = \frac{a(1+R_C+R_t) - R_t}{1 - (1 - 2a)(R_C + R_t)}$	<p><b>CASE 3</b></p> <p>LIMITS</p> $1/2 \leq a \leq 1$ $-(1 - R_C) \leq R_g \leq (1 + R_C)$	<p><b>CASE 4</b></p> <p>LIMITS</p> $1/2 \leq a \leq 1$ $\beta \leq (1-a)$
$\frac{P}{P_y} = \frac{[(R_C + R_g)(a - 2a\beta + \beta) - R_C + a - \beta]}{R_g}$	$\frac{P}{P_y} = \frac{1}{2} [(1+a) + 2a(R_C + R_g) - R_g]$	$\frac{P}{P_y} = \frac{1}{2} [(1-a) + 2a(R_C + R_g) - R_g]$	$\frac{P}{P_y} = \frac{1}{2} [(R_t + R_g) + 2a - \beta]$
$\frac{M_y}{M_y} = \frac{1}{2} (1+a + 2a^2)(1 + R_C + R_g) - R_C$ $+ R_t(a - 2a^2)$	$\frac{M_y}{M_y} = \frac{1}{2} (1-a + 2a^2)(1 + R_C + R_g) - R_g$ $+ (a+\beta) - 2(a-\beta)^2 - 2a\beta + 1$	$\frac{M_y}{M_y} = \frac{1}{2} [(1-a)(1+2a)(1+R_C + R_g) - R_g]$	$\frac{M_y}{M_y} = (1-a-\beta)(1+2a-4\beta) + 6\beta(1-\beta)$
$\frac{\phi}{\phi_y} = \frac{1 - R_C(1-2a) + R_g + 2aR_t}{2(1-a)}$	$\frac{\phi}{\phi_y} = \frac{1 + (a-\beta)(R_C + R_g) + 2R_t(1-a)}{1-a-\beta}$	$\frac{\phi}{\phi_y} = \frac{1 + (R_C + R_g)(1-a-\beta)}{1-a-\beta}$	$\frac{\phi}{\phi_y} = \frac{1 + (R_C + R_g)(1-a-\beta)}{1-a-\beta}$

Table 4  
SUMMARY OF TEST CONDITIONS

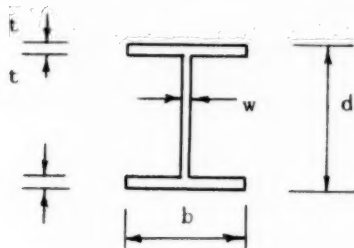
Test Number	Loading Conditions	Section	$\frac{P}{P_y}$	$\frac{L}{r}$	Type of Failure
T-3	b	8 WF 31	0.49	55	Pending and Twist
T-4	b	8 WF 31	0.12	55	Local Buckling
T-7	b	4 WF 13	0.27	111	Pending and Twist
T-9	b	4 WF 13	0.10	111	Pending and Twist
T-10	b	4 WF 13	0.51	111	Pending and Twist
T-12	c	8 WF 31	0.12	55	Pending and Twist
T-13	d	8 WF 31	0.12	55	Local Buckling
T-14	a	8 WF 31	0.12	55	(Was not carried to failure)
T-16	c	8 WF 31	0.12	41	Pending, Twist and Local Buckling
T-17	b	4 WF 13	0.12	55	Local Buckling
T-19	c	8 WF 31	0.12	27	Pending and Twist
T-20	c	4 WF 13	0.12	55	Pending and Twist
T-21	b	4 WF 13	0.50	55	Local Buckling
T-23	d	4 WF 13	0.12	84	Pending and Twist
T-24	b	4 WF 13	0.12	84	Pending, Twist and Local Buckling
T-26	c	4 WF 13	0.12	84	Pending and Twist



\* Slenderness Ratios Represent Free Lengths Between Knife-Edge  
(Based on measured cross-section dimensions)

Table 5

## Average Section Properties



	$d$	$b$	$w$	$t$	Area	$I_x$	$S_x$	$r_x$
--	-----	-----	-----	-----	------	-------	-------	-------

8 WF 31

Measured	8.069	8.032	0.299	0.427	9.177	111.356	27.60	3.483
Handbook	8.00	8.000	0.288	0.433	9.12	109.7	27.4	3.47
Variation, %	0.86	0.40	3.82	1.39	0.63	1.51	0.73	0.39

4 WF 13

Measured	4.139	4.140	0.258	0.337	3.759	11.215	5.419	1.727
Handbook	4.16	4.06	0.28	0.345	3.82	11.3	5.45	1.72
Variation, %	5.05	4.93	7.86	2.32	1.59	0.75	0.57	0.41

## Material Properties

Section	$\sigma_y$	E
8 WF 31	40.0 ksi	29,900 ksi
4 WF 13	39.5 ksi	29,200 ksi

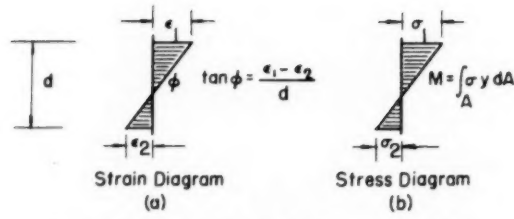


Fig. 1 Elastic Stress and Strain Distribution

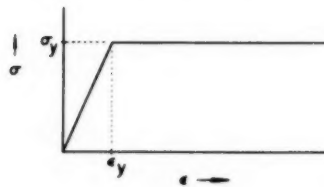


Fig. 2 Idealized Stress-Strain Diagram

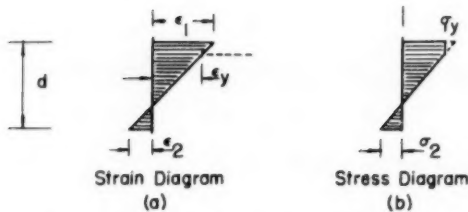


Fig. 3 Stress and Strain Distribution Patterns when Strain Exceeds the Elastic Limit

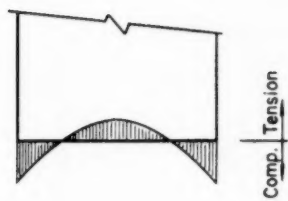


Fig. 4 Hypothetical Cooling Residual Stress Pattern  
for a Flat Plate

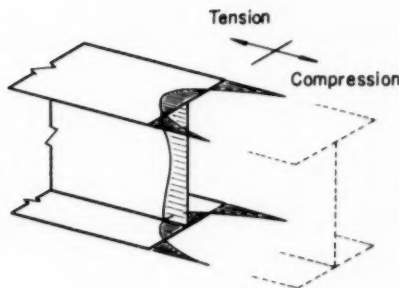


Fig. 5 Typical Cooling Residual Stress Pattern  
for a WF Section

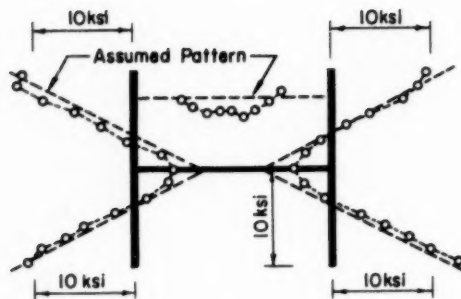


Fig. 6 Measured Residual Stress Pattern  
for the 8WF31 Section

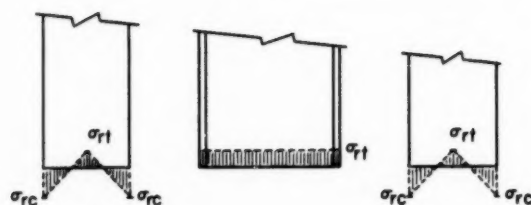


Fig. 7 Assumed Cooling Residual Stress Patterns  
for the Wide Flange Section

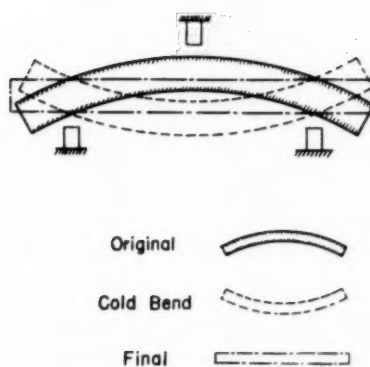


Fig.8 Diagrammatic Representation of the "Gag" used in Straightening Rolled WF Shapes

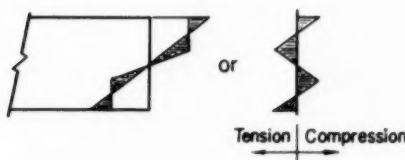


Fig.9 Residual Stress Pattern due to Cold Bending

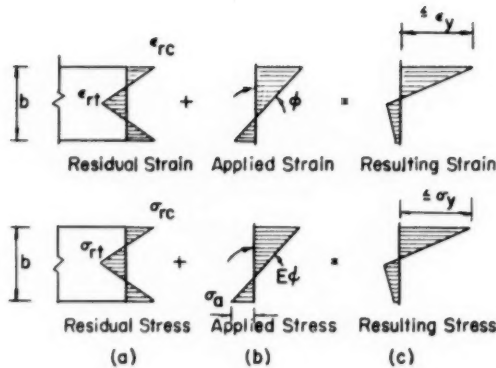


Fig.10 Influence of Cooling Residual Stresses on Elastic Stress and Strain Distribution (Plate Sections )

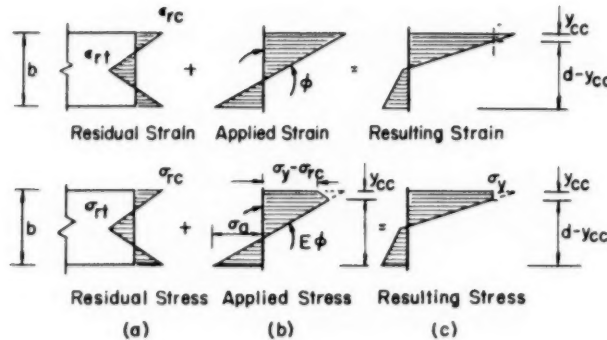
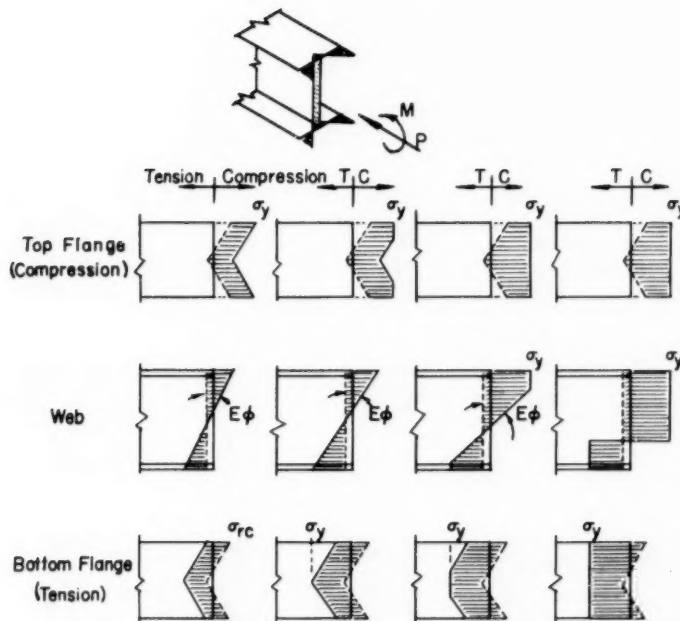


Fig.11 Influence of Cooling Residual Stresses on Stress and Strain Distribution when Strains Exceed the Elastic Limit (Plate Sections)

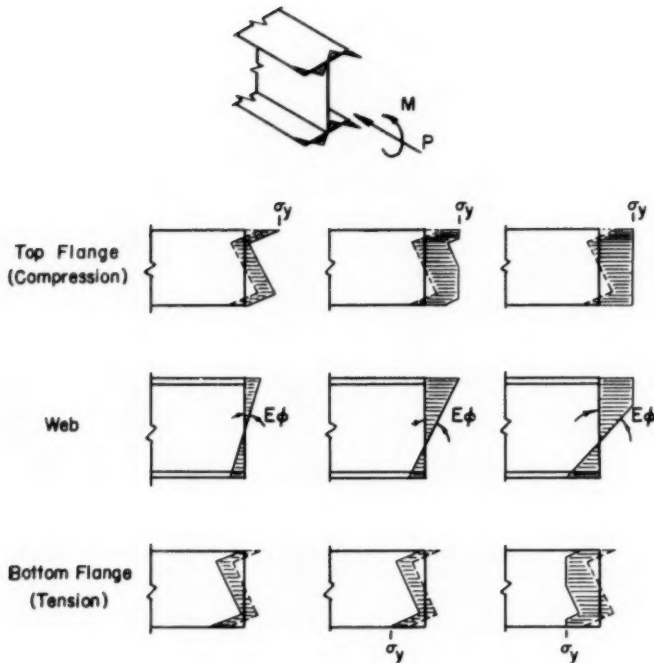


Comp. Flange	At Yield Point	Partial Yield	Complete Yield	Complete Yield
Tension Flange	Below Yield Pt.	At Yield Point	Partial Yield	Complete Yield

1.                   2.                   3.                   4.

Note: Applied Stress Patterns are Gross Hatched

Fig. 12 Influence of Cooling Residual Stress on Stress Distribution for WF Sections (Strong Axis Bending)



Comp. Flange	At Yield Point	Partially Yielded	Complete Yield
Tension Flange	Below Yield Point	At Yield Point	Partially Yielded

Note: Applied Stress Patterns are Cross Hatched

Fig.13 Influence of Cold Bending Residual Stress  
on Stress Distribution for WF Sections  
(Strong Axis Bending)

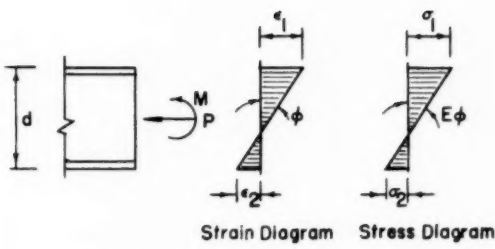


Fig. 14 Elastic Stress and Strain Diagrams

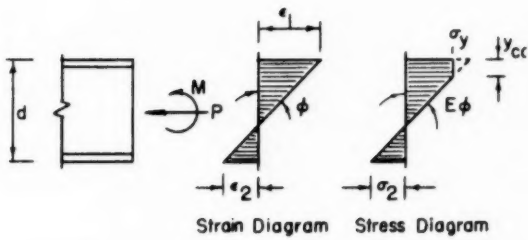


Fig. 15 Stress and Strain Diagrams  
when Strains Exceed the Elastic  
Limit

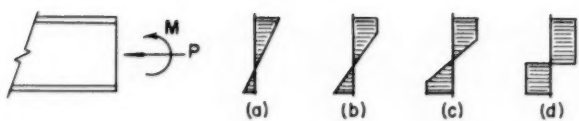


Fig. 16 Typical Progressive Yield Conditions  
Due to Beam-Column Loading

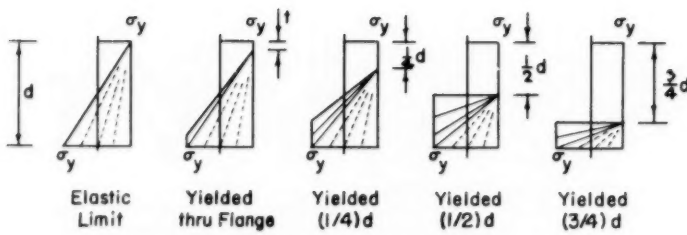


Fig. 17 Sample Set of Assumed Yield Penetration  
Conditions for Determination of Auxiliary  
M- $\phi$  and P- $\phi$  Curves

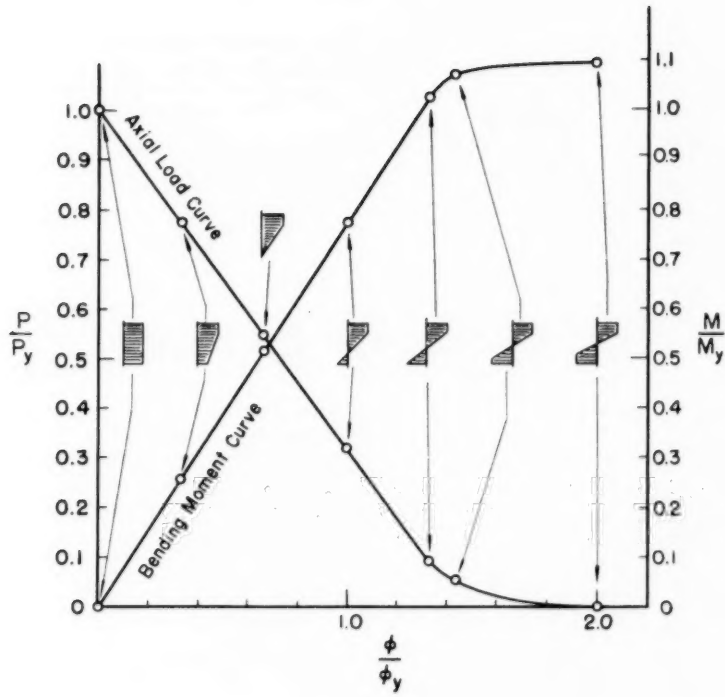


Fig. I8 Auxiliary  $M-\phi$  and  $P-\phi$  Curves for an Assumed Yield Penetration of  $1/4$  the Depth of the Section  
(8WF 3I)

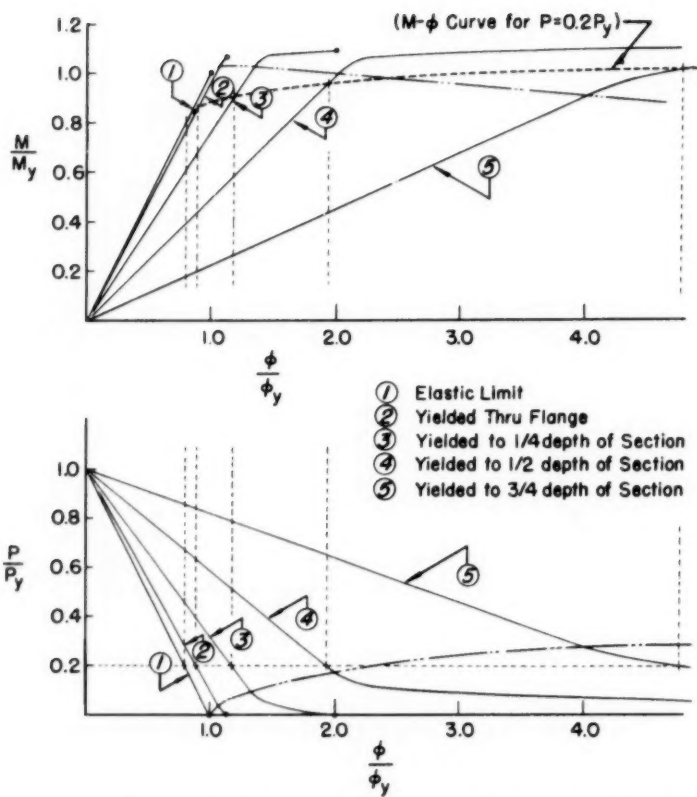


Fig.19 Typical Set of  $M-\phi$  and  $P-\phi$  "Auxiliary Curves"  
(8WF31)

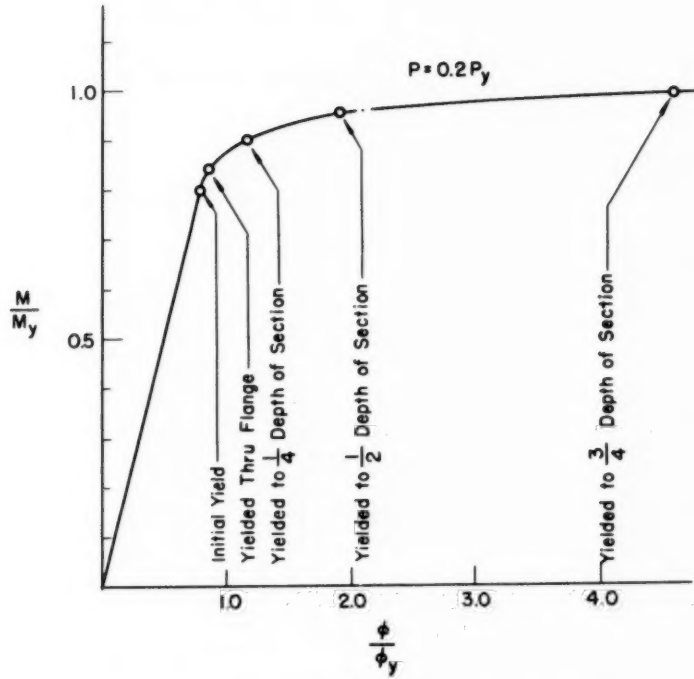


Fig.20 M- $\phi$  Curve for  $P=0.2 P_y$  (8WF31)

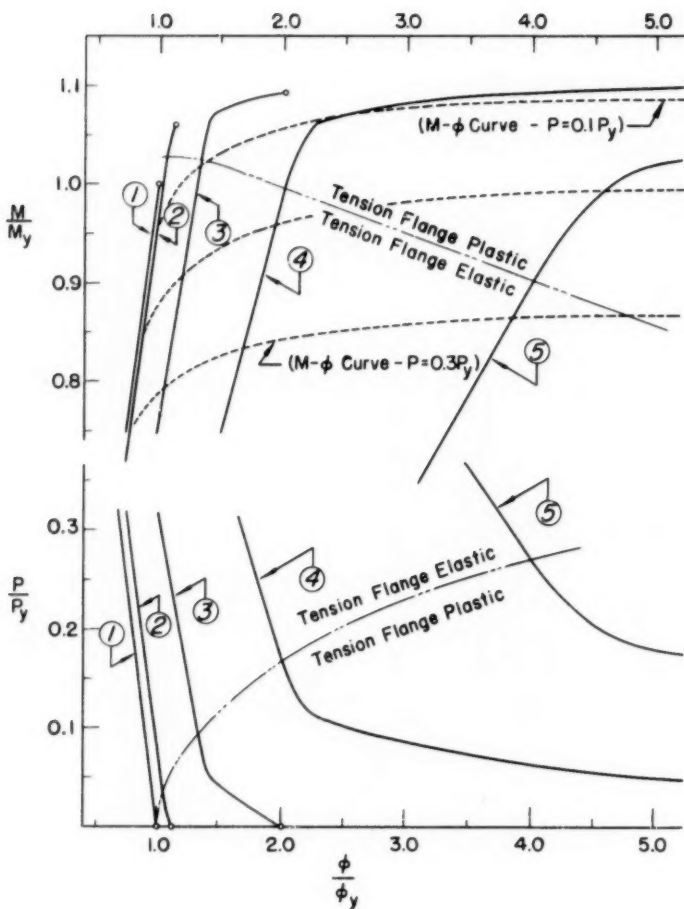


Fig. 21 Enlarged  $M-\phi$  and  $P-\phi$  "Auxiliary Curves"  
(8WF31)

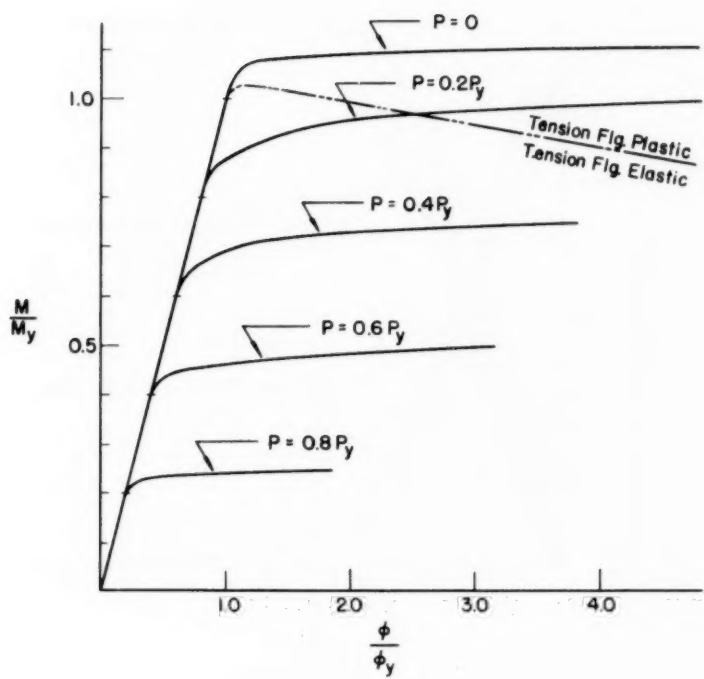


Fig.22 M- $\phi$  Curves for the 8WF3I Section  
(Strong Axis Bending)

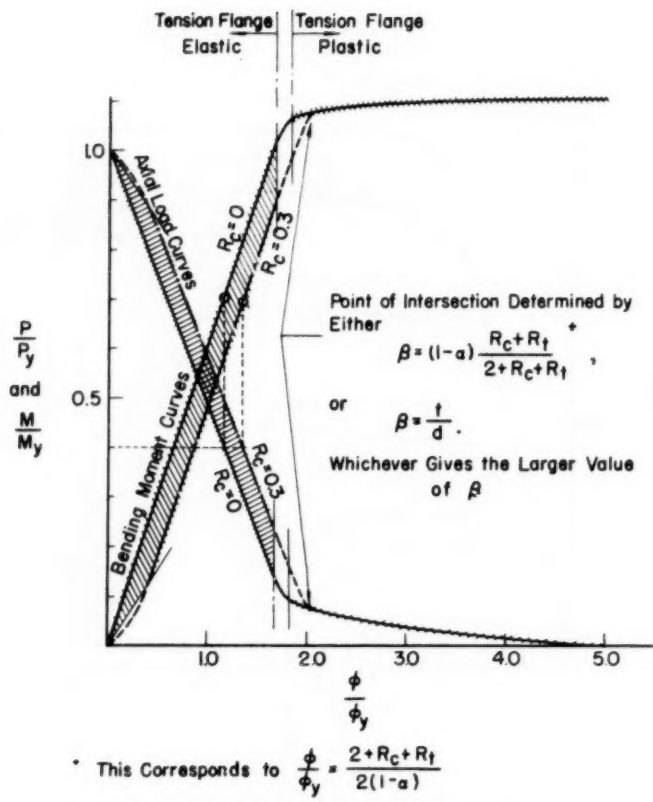


Fig. 23 "Auxiliary Curves" Including the Influence of Residual Stress  
 $(\alpha = 0.4, R_c = 0.3, 8WF31)$

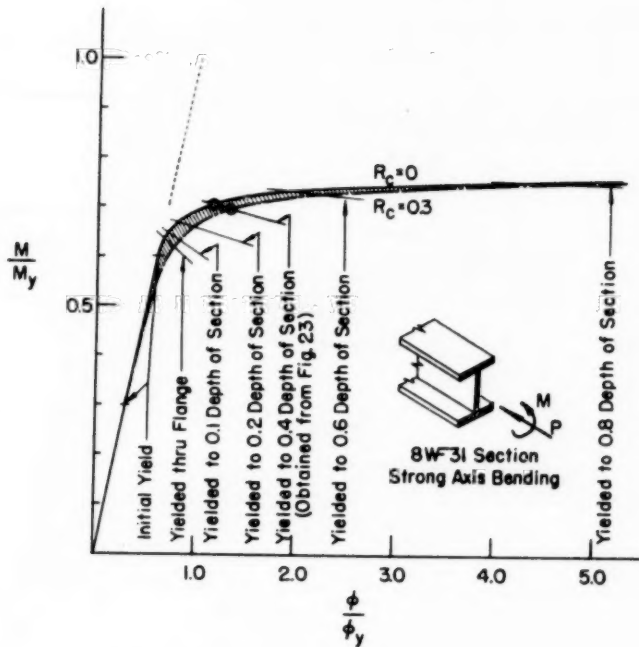


Fig. 24 M- $\phi$  Curve Including the Influence of  
Residual Stress for  $P = 0.4 P_y$   
(8WF3I)

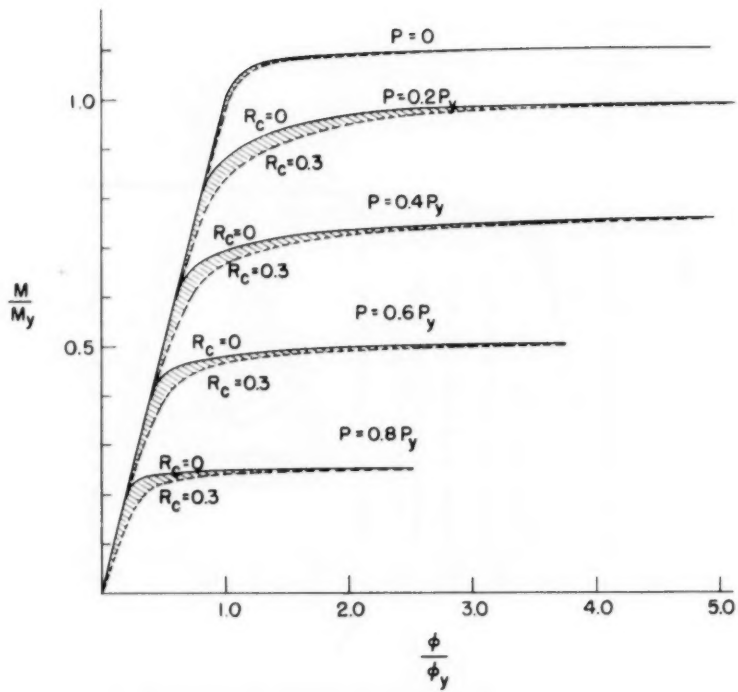


Fig. 25 M- $\phi$  Curves for the 8WF3I Including Residual Stress (Strong Axis Bending)

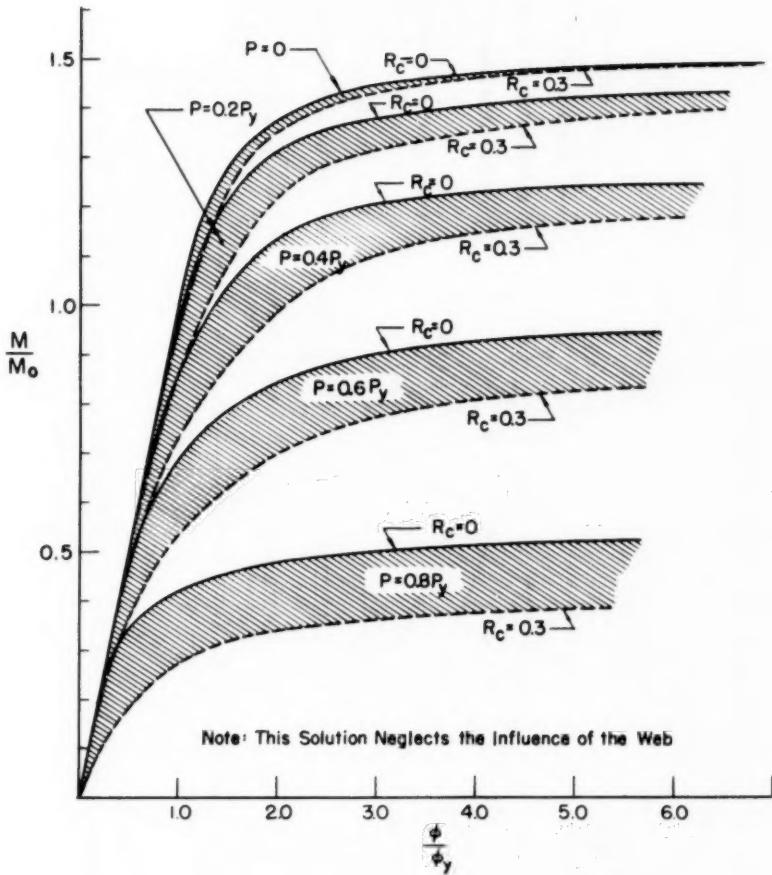


Fig.26 M- $\phi$  Curves for the 8WF3I Section Including Residual Stress  
(Weak Axis Solution)

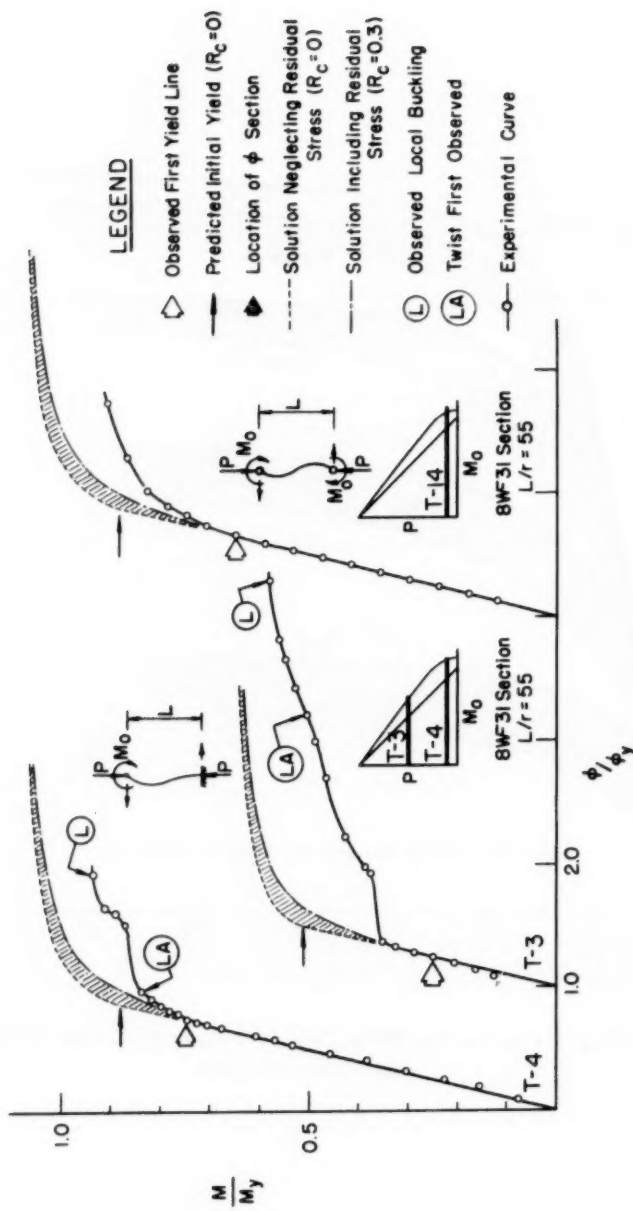


Fig.27 Experimental and Theoretical  $M-\phi$  Curves for Test Columns T-3, T-4 and T-14

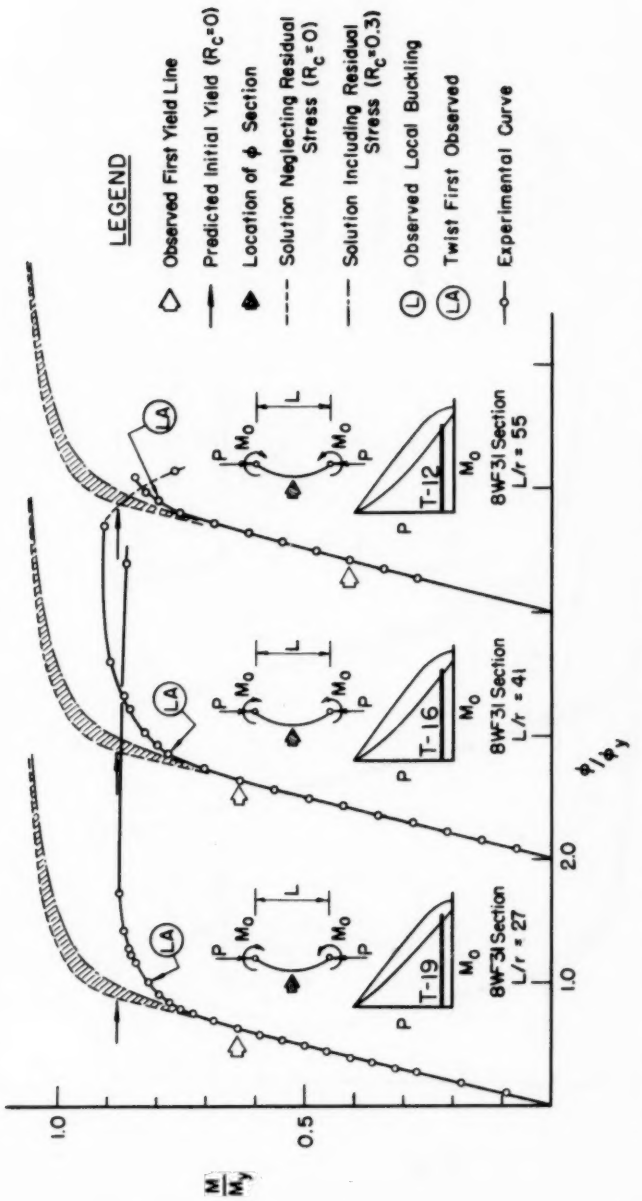


Fig.28 Experimental and Theoretical  $M-\phi$  Curves for Test Columns T-12, T-16 and T-19

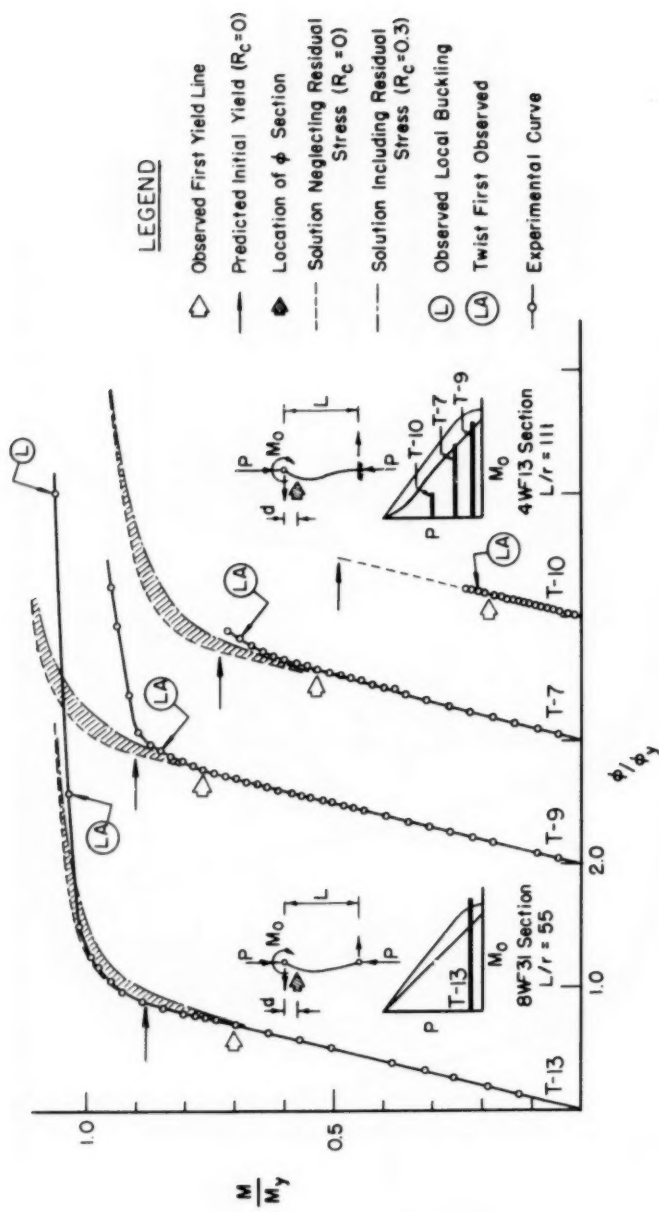


Fig.29 Experimental and Theoretical  $M-\phi$  Curves for Test Columns T-7, T-9, T-10 and T-13

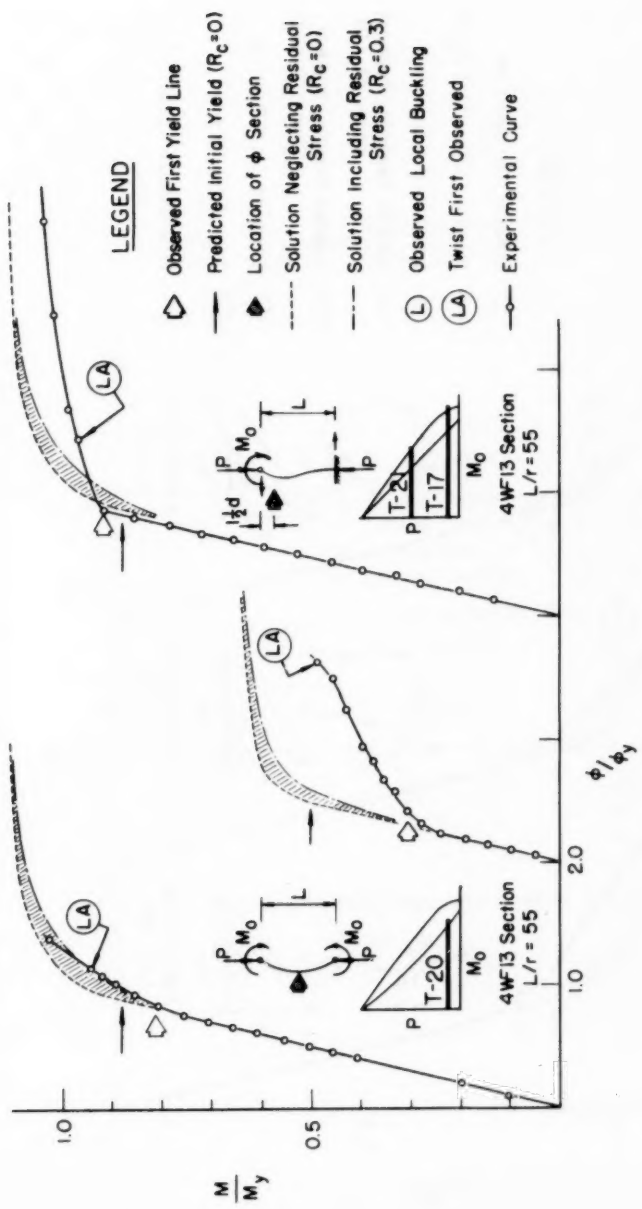


Fig. 30 Experimental and Theoretical  $M-\phi$  Curves for Test Columns T-17, T-20 and T-21

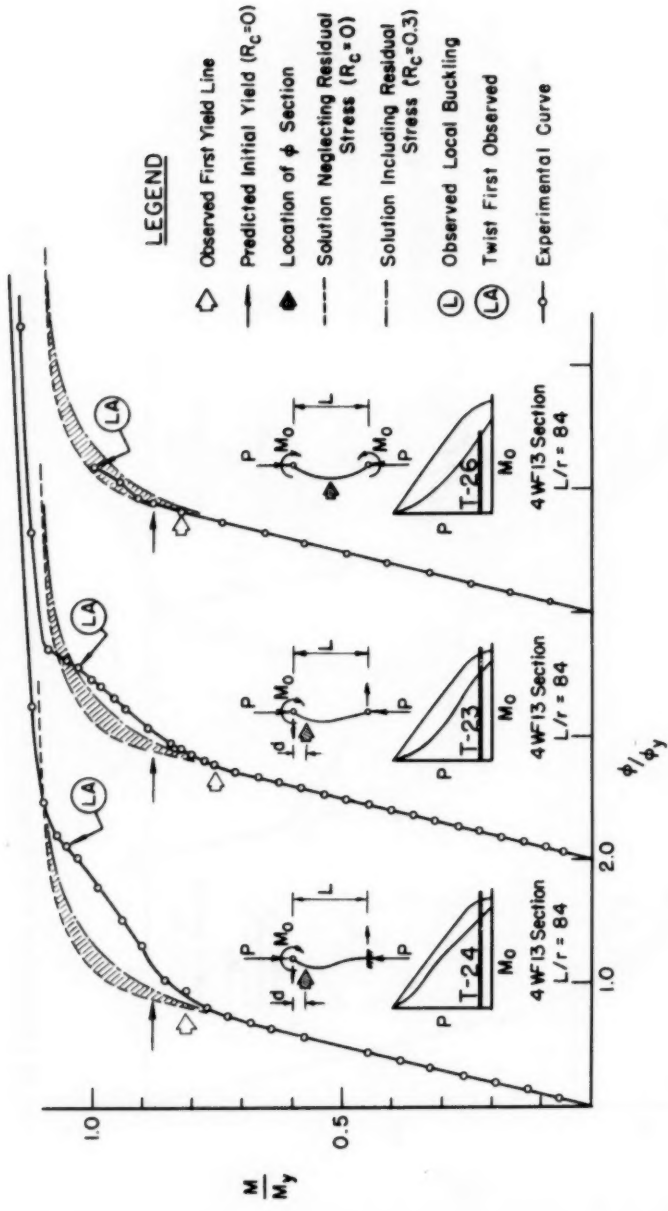


Fig.31 Experimental and Theoretical  $M-\phi$  Curves for Test Columns T-23, T-24 and T-26

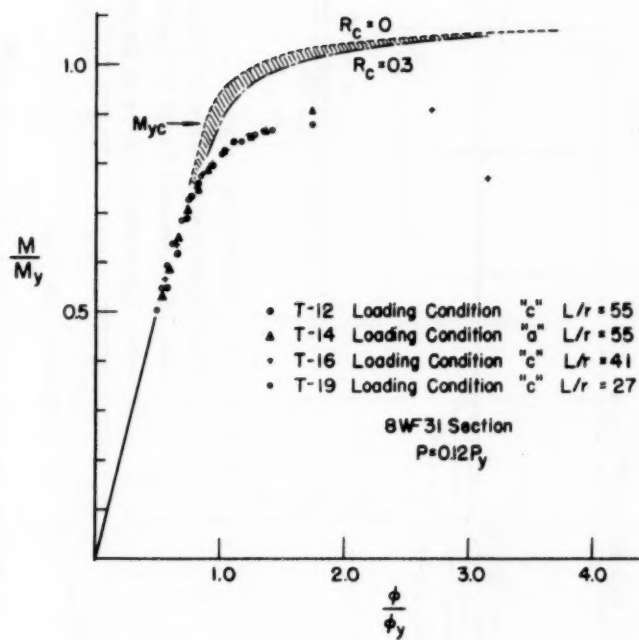


Fig.32 Experimental and Theoretical  $M-\phi$  Curves  
 - Summary -

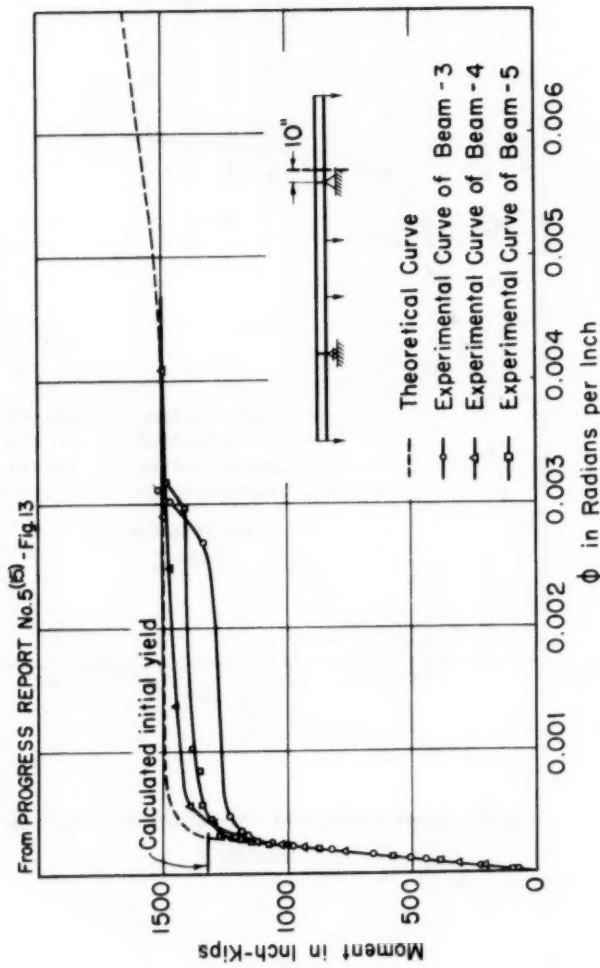


Fig. 33 Moment-Curvature Relation for a Continuous Beam(15)

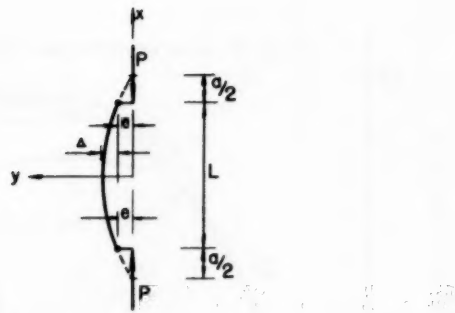


Fig. 34 Eccentrically Loaded Column

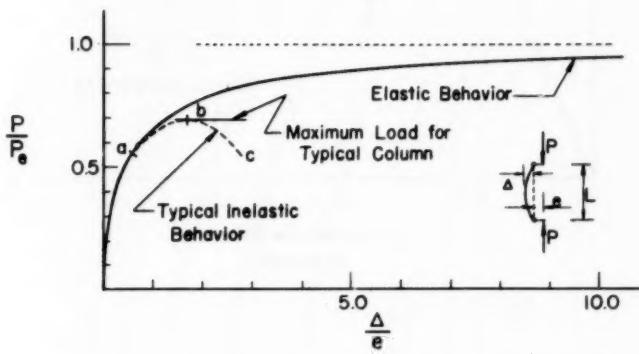


Fig. 36 Load-Deflection Relation for an Eccentrically Loaded Column

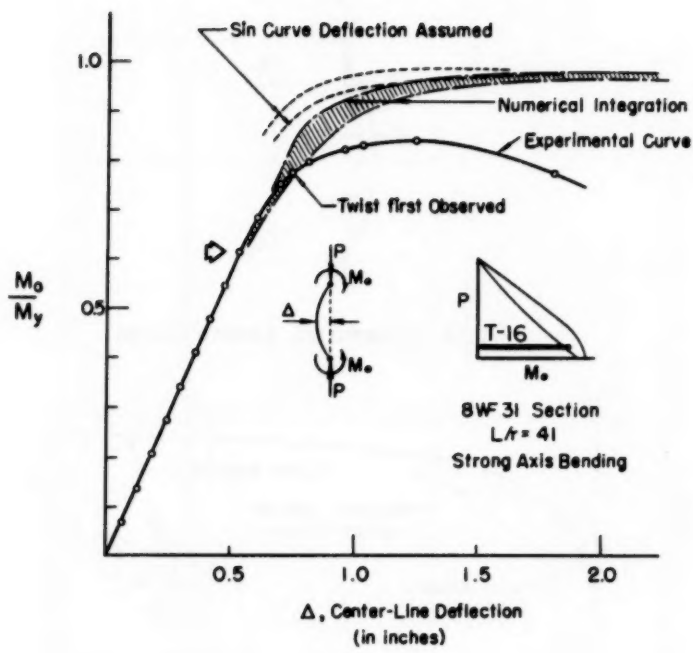


Fig. 35 Typical End-Moment vs Deflection Curves  
 (T - 16)

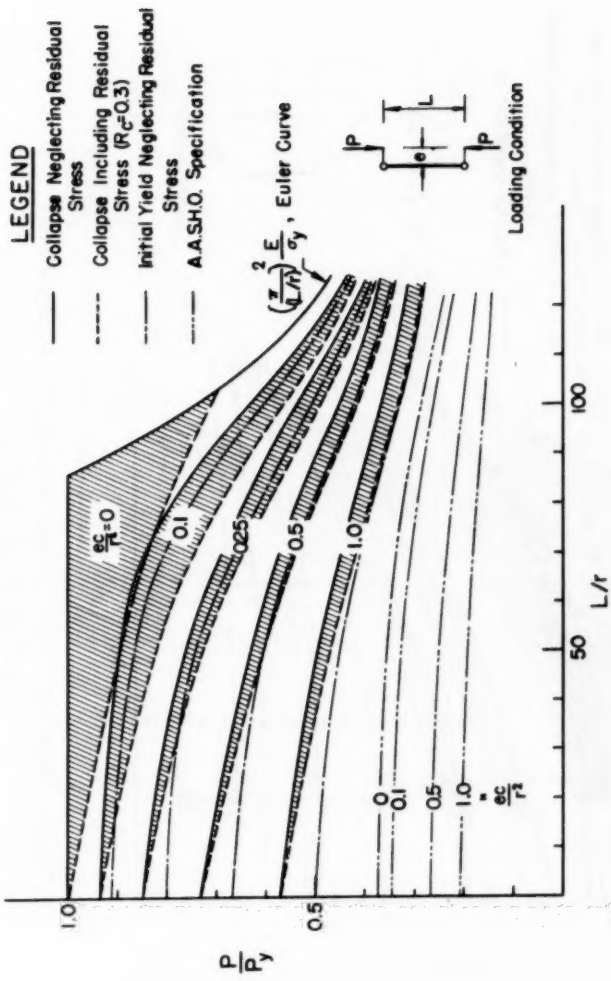


Fig. 37 Strong Axis Column Curves Including the Influence of Residual Stress ( $8WF31$ )

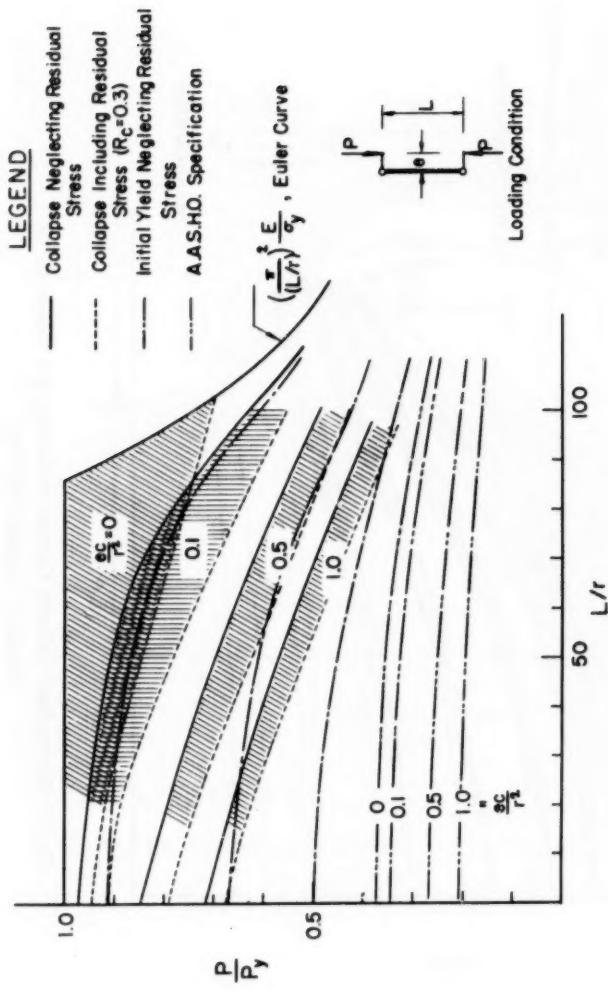


Fig. 38 Weak Axis Column Curves Including the Influence of Residual Stress (8WF31)

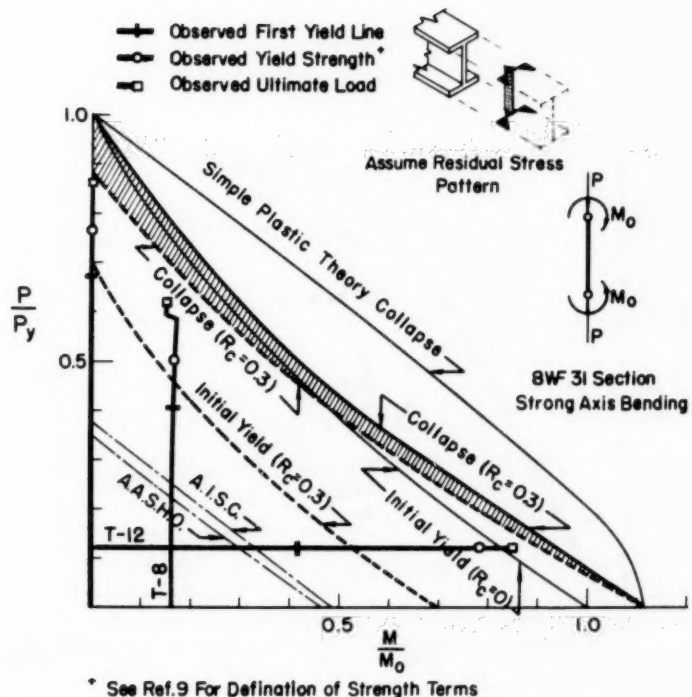


Fig. 39 Interaction Curves for 8WF 3I Section  
(Loading Condition "c",  $L/r = 55$ )

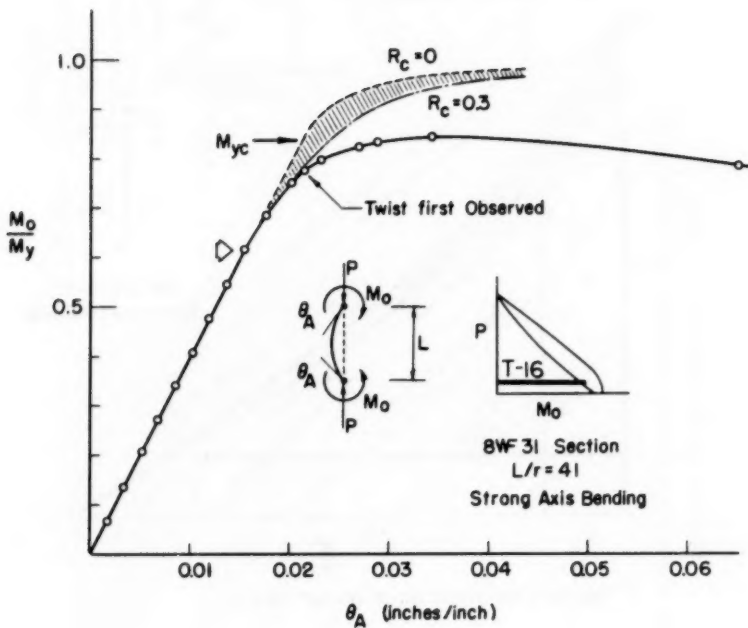


Fig. 40 Typical Curves of End Moment vs End Rotation (T-16)

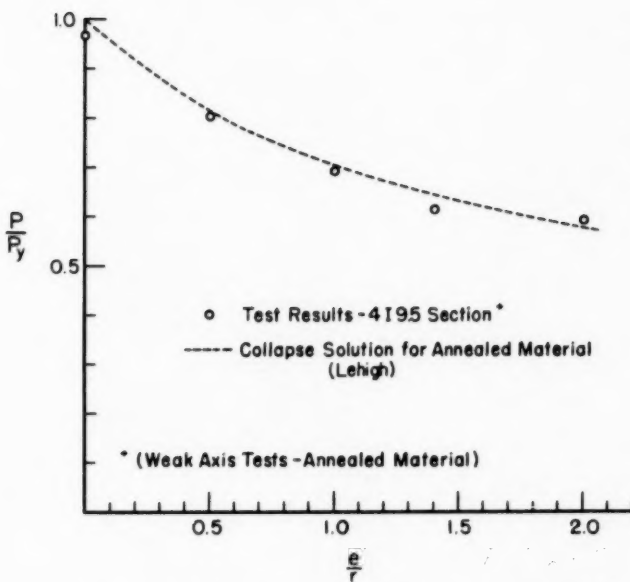


Fig. 41 Correlation Between Test Results (Cornell<sup>(14)</sup>) and Theoretical Analysis for 4I95 Members Bent About Weak Axis ( $L/r = 50$ )